

LAPPEENRANTA UNIVERSITY OF TECHNOLOGY  
Faculty of Technology  
Master's Degree Program in Technomathematics and Technical Physics

*Kulinskaya Natalia*

**NMR IN CRYSTALS AND POWDERS OF TOPAZES WITH  
DIFFERENT COLOURS**

Examiners: Professor Erkki Lahderanta  
Professor Vladimir Matveev

Supervisors: Professor Erkki Lahderanta  
Professor Vladimir Matveev

## **ABSTRACT**

Lappeenranta University of Technology  
Faculty of Technology  
Master's Degree Program in Technomathematics and Technical  
Physics

Kulminskaya Natalia

### **NMR in Crystals and Powders of Topazes with Different Colours**

Master's thesis

2009

45 pages, 21 figures, 4 tables

Examiners: Professor Erkki Lahderanta  
Professor Vladimir Matveev

Keywords: NMR, solid state, topaz, relaxation time, single crystal, quadrupolar splitting.

The present work is a part of the large project with purpose to investigate microstructure and electronic structure of natural topazes using NMR method. To reach this task we determined the relative contents of fluorine and hydrogen in crystals blue, colorless, wine and wine irradiated topazes. Then we determined the electric field gradients in site of aluminium atoms by NMR method, calculated EFG using ab initio method, and measured relaxation time dependence on heating temperature for blue, colorless, Swiss blue and sky blue topazes.

Nuclear magnetic resonance (NMR) is an effective method to investigate the local structure in the crystal. The NMR study of the single crystal gives detailed information especially about the local crystal structure.

As a result of this work we have received practical data, which is possible to use in future for making personal dosimetry and for preparation of mullite, which is widely used in traditional and advanced ceramic materials.

## TABLE OF CONTENTS

<b>INTRODUCTION.....</b>	<b>4</b>
<b>1. LITERATURE REVIEW .....</b>	<b>6</b>
1.1. Practice application of topaz.....	6
1.2. Physical Properties of Topaz .....	7
1.3. Crystal Structure.....	12
1.4. Influence of quadrupol interaction on NMR spectra.....	15
<b>2. EXPERIMENTAL PART .....</b>	<b>17</b>
2.1. Amount of fluorine and hydrogen atoms in crystals of a topaz measured by nuclear magnetic resonance method .....	17
2.2. Experimental definition of the component of electric field gradient tensor ...	20
2.3. The density functional theory .....	27
<b>3. SPIN-LATTICE RELAXATION TIME.....</b>	<b>38</b>
3.1. Theoretical background. ....	38
3.2. Experimental part .....	41
3.2.1. Sample preparation .....	41
3.2.2. The measurements .....	41
<b>CONCLUSIONS .....</b>	<b>48</b>
<b>REFERENCES.....</b>	<b>50</b>

## INTRODUCTION

One of the most interesting phenomenon nowadays is correlation between microstructure of the crystal and its physical properties. In particular, color of topazes ( $\text{Al}_2\text{SiO}_4(\text{OH}_x\text{F}_y)_2$ ) and their transparency in visible area of light are determined by the amount and the arrangement of defects, the color centers. The quantity and the quality of the defects is one of the typomorphic characteristics of various deposits. Color of crystals depend on the ratio between the amount of fluorine atoms and OH groups replacing fluorine, amount and sort of paramagnetic impurities, etc., and the defects formed by, for example, neutron or X-ray irradiation.

In the literature exist numerous studies on the structure and the properties of topaz  $\text{Al}_2\text{SiO}_4(\text{F},\text{OH})_2$ .

For more than fifty years the vibrational spectra of topaz, a solid solution of chemical formula  $\text{Al}_2\text{SiO}_4(\text{OH}_x\text{F}_{12x})_2$ , where  $0 < x < 0.3$ , have been a topic of intensive investigations using Raman and infrared spectroscopies. Most of these studies were related to the investigation of the symmetry of topaz as well as the OH/F substitution. Although no definitive answer has yet been established concerning the space group, much has been learned about the influence of the OH/F substitution on many of its physical properties such as, e.g., the refraction index and specific weight. On the other hand, much less is known about the relationship between the OH/F substitution and the concentration of color centers [1].

Investigation OH/F substitution, relation between the amount hydrogen and fluorine, and presence of paramagnetic impurities by method of a nuclear magnetic resonance, as far as we know, was not applied, though it is the most sensitive method.

The local structure and property of topaz strongly depend on the condition of the crystal formation and the treatment of the crystal.

Therefore, more information on the local and electronic structure of topaz obtained under several conditions is desirable. Nuclear magnetic resonance (NMR) of nuclei with spin  $I > 1/2$  is an effective method to investigate the local structure in the crystal, since the quadrupole interaction is very sensitive to the environment of the observed nuclei [23, 24]. The NMR study of the single crystal gives detailed information especially about the local structure in the crystal from the tensor of the electric field gradient (EFG) which is the second rank tensor determined by the principal values and the directions of the principal axes.

The purpose of this work is to use NMR method to study microstructure and electronic structure of topaz mineral: crystals blue, colorless, Swiss blue, sky blue, wine and wine irradiated. To reach this task we defined the relative contents of fluorine and hydrogen in crystals blue, colorless, wine and wine irradiated topazes. Then we determined the electric field gradients in site of aluminium atoms by NMR method, calculated EFG by ab initio method, and measured relaxation time dependence on burning temperature for blue, colorless, Swiss blue and sky blue topazes.

# **1. LITERATURE REVIEW**

## ***1.1. Practice application of topaz***

The most important use of topaz is as a gemstone. It is one of the most popular and widely used gemstones in jewelry, and has been used that way for centuries. The mineral is almost always found in the form of large, well developed crystals. There are specimens of topaz that have been found weighing up to several hundred kilograms. Gems have been cut from huge crystals which are several thousands of carats, such as a 144,000 carat golden brown topaz shown at the 1974 National Gem and Mineral show in Lincoln, Nebraska; and a 36,853 carat champagne topaz carved in 1989. Most of these large topaz deposits are found in Brazil.

Topaz is one the hardest minerals, and is the hardest silicate mineral, with Mohs hardness equal to eight. This feature is undermined by the fact that it has perfect basal cleavage in one direction. This makes it difficult to cut and polish, and therefore carvings made out of topaz are very rare.

It is still valuable as a gemstone, however, because of its high luster, good crystal form with many facets, and good color. It comes in many colors ranging from colorless to red, pink, yellow, orange, brown, and pale blue. Its colorless variety is fairly common, and can be cut to look like diamond, or heat-irradiated to turn it into blue topaz. This has become a very popular, less expensive substitute for aquamarine. The orange-yellow variety, most characteristic of the mineral, is called "imperial topaz," and is the most valuable form. Prices for imperial topaz range from \$50-\$400 per carat. Prices for blue topaz are around \$0.75-\$10.00 per carat.

Besides its value as gemstone the optical and piezoelectric properties of natural topaz makes it an interesting material for technological applications. Recent studies reveal that the thermo

luminescent (TL) characteristics of topaz make it suitable for dosimetry. In the work [2] it was indicated that the colorless topaz from Minas Gerais, Brazil, is a promising material for dosimetric application. It can be useful for personal dosimetry, in monitoring the radiation sources usually employed in radiotherapy, and in the dosimetry of nuclear accident, where sometimes we want to know which kind of material can be used to measure the radiation dose in the region of the accident during or after the accident.

Topaz mineral is used for preparation of mullite, which is widely used in traditional and advanced ceramic materials due to its low thermal expansion, low thermal conductivity, and excellent creep resistance. This is a very attractive option, since high-purity colorless topaz is abundant in nature and its gemological or commercial value is low. Moreover, the transformation of topaz to mullite is clean procedure which does not form chemical residues, in line with the principles Green Chemistry.

Topaz is system that has been found to be stable at high pressures up to those of the lower mantle, and thus may be important in the siliceous sediments of subducting slab [3].

### ***1.2. Physical Properties of Topaz***

Topaz,  $\text{Al}_2\text{SiO}_4(\text{F},\text{OH})_2$ , is one of the most important F/OH-bearing silicates, found in different geological environments: as accessory mineral in F-rich granitic rocks, associated to pneumatolithic/hydrothermal events [4 — 7]. The crystal structure of topaz was first solved by Alston and West (1928) and Pauling (1928) [8, 9]. Later, several studies have been devoted to the crystal chemistry and physics of topaz along the solid solution  $\text{Al}_2\text{SiO}_4\text{F}_2$ – $\text{Al}_2\text{SiO}_4(\text{OH})_2$  [8 — 23]. For natural topazes, with  $\text{OH}/(\text{OH}+\text{F}) < 0.5$ ,

the crystal structure is described by the Pbnm space group, with one H-site (Fig. 1).

In contrast, the crystal structure of the synthetic  $\text{Al}_2\text{SiO}_4(\text{OH})_2$  end-member contains two non equivalent and partially occupied (50%) H-sites and some evidence for a lower symmetry (Pbn2<sub>1</sub> space group) has been reported by Northrup et al. 1994 and Chen et al. 2005 [18, 23]. The thermal expansion of topaz was first described by Skinner [24] by means of in situ X-ray powder diffraction. Later, the thermal and pressure behaviour of a natural topaz ( $\text{Al}_{2.01}\text{Si}_{1.00}\text{O}_4\text{F}_{1.57}(\text{OH})_{0.43}$ ) was investigated by Komatsu et al. [25] by means of in situ X-ray single-crystal diffraction. The high pressure-lattice parameters have been measured up to about 6.8 GPa. The bulk modulus has been calculated on the basis of the volume data collected up to 6.2 GPa with a truncated second-order Birch-Murnaghan equation-of-state (II-BM-EoS, Birch 1947) [26], i.e. with the bulk modulus value fixed to 4. The calculated bulk modulus, 154 GPa, significantly differs from the elastic stiffness, 174.3 GPa, obtained for a natural topaz.

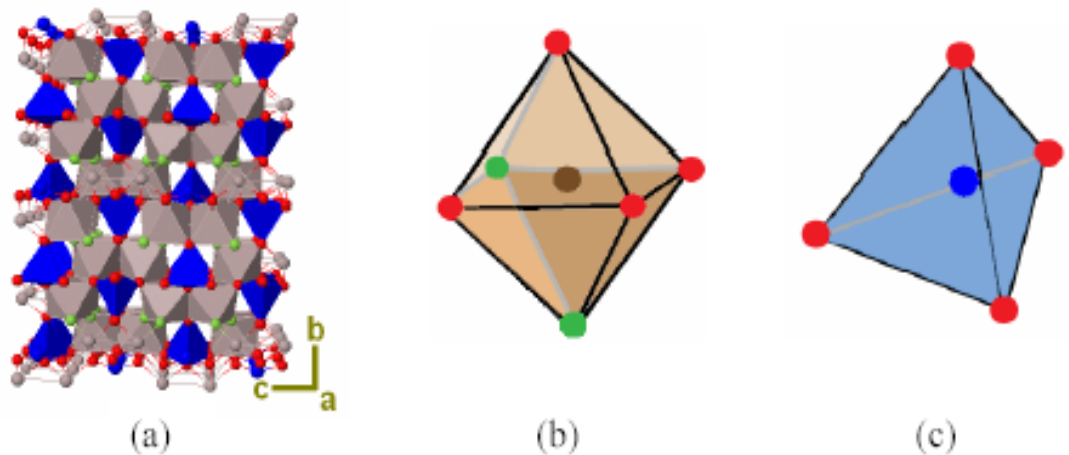


*Fig. 1. The crystal structure of Topaz: (a) Topaz has an orthorhombic crystal structure. The chains of aluminum octahedral are normal to the c axis. (b) Aluminum octahedral has 1 aluminum atom, 4 oxygen atoms, and 2 fluorine/hydroxyl atoms. (c) Silica tetrahedral has 1 silica atoms and 4 oxygen atoms.*

Topaz is an orthorhombic mineral. This means that in crystal lattice, each unit cell is shaped like a rectangle. In crystallography the unit cell sides are named  $a$ ,  $b$  and  $c$ , with  $a$  being the side that comes out towards you,  $b$  being the side that goes to right, and  $c$  being the side that goes up. In cube  $a = b = c$ , but in an orthorhombic mineral  $a \neq b \neq c$ . However, all the angles are  $90^\circ$  like in a cube [27].

Because the length, width and height of each unit cell are different, topaz has three refractive indices. A refractive index is a number that represents how much light is slowed down as it passes through a substance. The higher the number, the more the light is slowed down. The refractive index for air is 1, and for water is 1.53. If material has more than one refractive index, it means that in such material light will travel at different velocities depending on direction. The refractive indices for topaz in directions  $a$ ,  $b$  and  $c$  are  $n_a = 1.606 - 1.634$ ,  $n_b = 1.609 - 1.637$ , and  $n_c = 1.616 - 1.644$  respectively. The refractive index for light traveling along  $c$  is highest, because  $c$  is the longest edge. The light has to travel through more material going in  $c$  direction, so it gets slowed down more.

These refractive indices are given in a range, instead of just as one number, because they vary depending on how much OH exist in the topaz. The chemical formula for topaz is  $\text{Al}_2[\text{SiO}_4](\text{OH},\text{F})_2$ . The comma between OH and F means that hydroxyl can be interchanged with fluorine in the lattice and the mineral will still be topaz. The more hydroxyl there is the higher the refractive indices will be.

The birefringence of topaz is  $0.008 - 0.011$ . Birefringence is simply the difference between the highest refractive index and the lowest refractive index. The birefringence for topaz is rather low compared to that of other minerals.

Topaz is biaxial mineral. This means it has two optical axes. An optical axis is a special line that when you cut the mineral exactly perpendicular to it (so that you are looking straight down it when you look at a thin section of the mineral), the two sides of the unit cell in the plane directly below you will be equal, and light will be slowed down by the same amount in every direction (all refractive indices will be similar). The angle between these two optical axes varies with different biaxial minerals, and is called  $2V$ . For topaz  $2V = 48 - 68^\circ$ . The angle is smaller if there is more OH is in the mineral.

Topaz is also designated as being biaxial "positive," instead of biaxial negative. Being biaxial positive means that the acute part of the  $2V$  angle is bisected by the  $Z$  axis (which is the axis upward in the  $c$  direction). A biaxial negative mineral would have the acute angle between its optic axes bisected by the  $X$  axis (the axis to the right in the  $b$  direction).

Topaz has density of  $3.49 - 3.57 \text{ g/cm}^3$  and it is lighter when it has more OH. This range is about average density for minerals. The density of quartz, an average mineral, is  $2.65 \text{ g/cm}^3$ .

Topaz has Mohs hardness of 8, which makes it one of the hardest minerals. Mohs hardness for minerals is reported on a scale of 1 to 10 with the hardest mineral (diamond) being 10 and the softest (Talc) being 1. Glass has a hardness of 5.5. A mineral can only scratch something less hard than it, and can only be scratched by something harder than it.

Topaz has perfect cleavage in the (001) plane, which is the plane that is pierced through by  $c$  but not by  $a$  or  $b$  – in other words, the plane perpendicular to  $c$ . This means that its bonds have natural weakness in  $c$  – direction, and it breaks easily and smoothly along (001). This kind of cleavage is also called basal cleavage.

Topaz is an orthosilicate, which means it is composed of isolated silica tetrahedral. A silica tetrahedron  $\text{SiO}_4$  molecule that has one silicon atom in the middle surrounded by four oxygen atoms sticking out at  $119^\circ$  to each other, making up the four corners of a tetrahedron. Silica tetrahedral is the building blocks of all the silicate minerals. In topaz, these tetrahedral do not touch each other directly, but are surrounded by Al atoms which bond to the O atoms in the silica tetrahedral as well as to (OH) or F ions.

The main features of topaz when compared with other minerals are its hardness, cleavage, low birefringence, positive optical sign and moderate  $2V$  angle. In addition, it shows high relief, which means its edges stand out distinctly from the surroundings when it is viewed under a microscope. It can be pleochroic, which means it changes color when it is rotated under the microscope.

The mineral is also distinguished by the fact that its cleavage trace is parallel to the fast ray. Under the microscope, minerals will have dark straight lines going in the direction of their cleavage. These lines are called the cleavage trace. When light enters any mineral, it is split into two rays, and one travels faster than another. The direction of the fast ray is an optical property of a mineral. In topaz, this ray travels parallel to the cleavage trace.

These properties allow topaz to be distinguished from similar minerals like andalusite, melilite, vesuvianite, quartz and feldspars.

NMR method was used only a little for studies of topaz. The angular dependence of the  $^{27}\text{Al}$  NMR spectrum was measured for single crystals of smoky and colorless topaz,  $\text{Al}_2\text{SiO}_4(\text{F},\text{OH})_2$ . Smoky topaz was obtained by irradiating high energy neutrons to colorless topaz. The quadrupole coupling constant  $e^2Qq/h$  and the asymmetry parameter  $\eta$  were obtained from the analysis of the angular dependences of quadrupole splitting of the  $^{27}\text{Al}$  NMR spectrum. The

local structures around the aluminum atoms in smoky and colorless topaz were discussed based on the magnitude and the direction of the electric field gradient (EFG). The directions of principal axes of the EFG tensor of  $^{27}\text{Al}$  were close to the directions of Al – O and Al – F bonds. The difference in the bond lengths between Al(1) – F(1) and Al(1) – F(2) was found to affect the  $x$  and  $y$  components of the EFG tensor.

For topaz – OH the  $^1\text{H}$  MAS NMR (magic angle spinning of nuclear magnetic resonance) spectra contain an asymmetric peak with maximum at 4.1 ppm and a tail at higher frequency, suggesting the presence of more than one H local environments, all with relatively weak hydrogen bonding. The  $^1\text{H}$  –  $^{29}\text{Si}$  CP (cross polarization) MAS NMR spectra show an asymmetric peak with a maximum near –83.3 ppm and a tail at higher frequency. Because there is only one unique Si site in the reported crystal structure (Wunder et al.,1993) [19], this is indicative of structural disorder in topaz – OH that may be related to the H distribution.

### ***1.3. Crystal Structure***

The crystal structure of topaz was determined independently by Alston and West [8] and Pauling [9]. The topaz structure is made up of silica tetrahedral and aluminum octahedral. Topaz is a nesosilicate (orthosilicate). In nesosilicate structure, the tetrahedral do not share oxygen with other tetrahedral. In the case of topaz, the silica tetrahedral shares each of their oxygen with aluminum octahedral [31]. The aluminum octahedral are joined by shared edges (edges with 2 oxygen) creating kinked chains normal to the  $c$  axis, meaning  $z$  crystallographic axis. This arrangement creates alternating close-

packed layers of O, F and O normal to the *b* axis. Topaz belongs to the orthorhombic crystal system. It is in the space group Pbnm. Topaz has Pbnm space group when the fluorine-hydroxyl sites are equivalent and the structure is disordered. Ordering in relation to hydroxyl content was suggested by Akizuki et al. (1979) [12] to explain anomalous optical properties in some topaz.

There parameters of the unit cells and atomic positions are different for natural topazes with different deposit (see Table 1)

Tabl.1

Parameters of the unit cell	$Al_2SiO_4F_2$	$Al_2SiO_4(OH)_2$
$a(\text{\AA})$	4.652	4.720
$b(\text{\AA})$	8.801	8.920
$c(\text{\AA})$	8.404	8.418

The structural data obtained in work [2] by X-ray spectroscopy have been used in this work for calculation EFG and distributions of electronic density in crystals of a topaz ( $Al_2SiO_4F_2$ ). The lattice parameters of this structure are:

$$a = 8.8116 \pm 0.0002 \overset{0}{\text{\AA}} \quad b = 16.6946 \pm 0.0004 \overset{0}{\text{\AA}} \quad c = 15.8481 \pm 0.0003 \overset{0}{\text{\AA}}$$

Positions of basic atoms also are presented in Table 2.

Tabl.2

index	atom	valence	x	y	z
1	Al(8a)	$Al^{3+}$	0.9047	0.1309	0.0817
2	O(4c)	$O^{2-}$	0.7963	0.5321	0.25
3	F(8a)	$F^{1-}$	0.9006	0.7533	0.0599
4	Si(4c)	$Si^{4+}$	0.4005	0.9409	0.25
5	O(4c)	$O^{2-}$	0.4531	0.7559	0.25
6	O(8a)	$O^{2-}$	0.7904	0.0108	0.9069

### ***Trace Elements***

Generally, topaz has only few trace elements. Germanium substituting for Si has concentration in the range of 200 – 400 ppm. Cr substituting for Al, can range in concentration from 20 ppm to 500 ppm. Mn usually has concentrations less than 30 ppm. For the elements B, Li, and Na concentrations of > 100 ppm have been reported but normal ranges for these elements are 40 – 60 ppm. Other elements found in topaz include Nickel (80 ppm), V (< 20 ppm), and Cobalt (< 8 ppm). Radiogenic helium was reported in topaz obtained from Volyn region of Ukraine [31].

### ***F-OH substitution***

Isovalent isomorphism is observed between F and OH ions, and their relative amounts in different crystals can strongly vary. The difference between relative contents of ions is one of the reasons why topazes form with different colors. It is still a question whether hydrogen enters into hydroxyl's structure or replaces atoms of fluorine in crystal lattice. Ratio between amount of fluorine and hydrogen can be defined from relations between integral intensities on NMR spectra.

In solid-state physics, the electric field gradient (EFG) measures the electric field gradient at an atomic nucleus generated by the electric charge distribution and the other nuclei. The EFG couples with the nuclear electric quadrupole moment of quadrupolar nuclei (those with spin quantum number more than half) to generate an effect which can be measured using nuclear magnetic resonance (NMR). EFGs are highly sensitive to the electric density in the immediate vicinity of a nucleus. This sensitivity has been used to study influence of substitution, weak interactions, and charge transfer on charge distribution.

#### 1.4. Influence of quadrupol interaction on NMR spectra

Nucleus, which have spin  $I > \frac{1}{2}$  do not have spherical symmetry; therefore their charge density distribution should be described using multipole moments of a different rank. As it is known, charge distribution inside the nucleus is characterized by the center of inversion and it cannot have vectors properties and, hence, nucleus cannot have dipole electric moment and other uneven moments of higher order. This is proved by experiment.

The electric moment of a nucleus is *quadrupole moment*. If a particle or system of particles have symmetry axes it means that the main axes of any tensor, will be directed on symmetry axes, and the tensor itself will have a diagonal form. Tensor of quadrupole moment of nucleus in coordinate system which  $z$ -axis coinciding with direction a symmetry axis of the infinite order  $C_\infty$ , and two other coordinate axes with direction of two mutually perpendicular axes of symmetry of the second order, axis-symmetric ( $eQ_{xx}^* = eQ_{yy}^*$ ) and diagonal:

$$eQ^* = \begin{pmatrix} eQ_{xx}^* & 0 & 0 \\ 0 & eQ_{xx}^* & 0 \\ 0 & 0 & eQ_{zz}^* \end{pmatrix}. \quad (1)$$

The sum of diagonal members of the tensor of quadrupole moment is zero:

$$eQ_{xx}^* + eQ_{yy}^* + eQ_{zz}^* = 0, \quad (2)$$

The magnitude  $eQ_{zz}^*$  determines the deviation of density distribution of a charge inside the nucleus from spherical symmetry.

A nucleus in the condensed matter is in environment of electrical charged particles such as other nuclei and electrons. These charges create non-uniform local fields. Because the nucleus sizes are

small in comparison with distances to the nearest charged particles, its interaction with environment can be presented as interaction nuclear quadrupole moments. Coulomb interaction energy of nuclear charge with intracrystalline electric field corresponds to an optical frequencies not get in frequencies considered in a nuclear magnetic resonance. Thus, interaction between nuclei with the electric fields created by the neighbours, can be described like interaction between nuclear quadrupole electric moments with field gradients.

Effective Hamiltonian of quadrupole interactions in the coordinate system connected with the main tensor axes of an electric field gradient can be written in the form

$$\hat{H}_Q = \frac{e^2 q Q}{4I(2I-1)} (3\hat{I}_z^2 - \hat{I}^2 + \frac{\eta}{2} (\hat{I}_+^2 - \hat{I}_-^2)). \quad (3)$$

$V_{zz}$  is *main component of an electric field gradient* and is designated by  $eq$ , and  $|V_{xx} - V_{yy}| / |V_{zz}|$  is *asymmetry parameter* and is indicated through  $\eta$ . Knowing the components of electric field gradient it is possible to define electric structure of a crystal, using not empirical calculation methods.

Experimental value of the tensor of electric field gradients can be obtained from spectra of a nuclear magnetic resonance, using a method of single rotation of a crystal in a magnetic field.

First order perturbation theory gives  $2I$ , the magnetic resonance frequencies, and for crystal with axial symmetry we have:

$$\nu_{m+1 \rightarrow m} = \nu_0 + (3A/h) [(3/2) \cos^2 \theta - \frac{1}{2}] (2m+1), \quad (4)$$

where  $\nu_0 = -\gamma H_0 / (2\pi)$  is the resonance frequency without the quadrupolar perturbation,  $A = e^2 q Q [4I(2I-1)]^{-1}$  is the quadrupolar coupling constant, and  $\theta$  is the angle between the main axis  $z$  of EFG tensor and  $H_0$ .

## 2. EXPERIMENTAL PART

### 2.1. Amount of fluorine and hydrogen atoms in crystals of a topaz measured by nuclear magnetic resonance method

Using nuclear magnetic resonance (NMR) were investigated four topaz samples: wine, wine irradiated, blue and colorless. Spectra on nuclei  $^1\text{H}$  and  $^{19}\text{F}$  have been measured on a spectrometer of wide lines ПЯ-2301 with two methods, in the first way frequency of the generator remained constant and the magnetic field changed, in the second way the magnetic field was constant and frequency was changed. Ratio of integral intensities did not change within the limits of error. The axis "c" is parallel to the external magnetic field for all NMR spectra. The modulation amplitude was 2.2 Gs. Because of small intensity of NMR spectra on nuclei of hydrogen  $^1\text{H}$ , each spectrum was recorded 4 times and results were averaged.

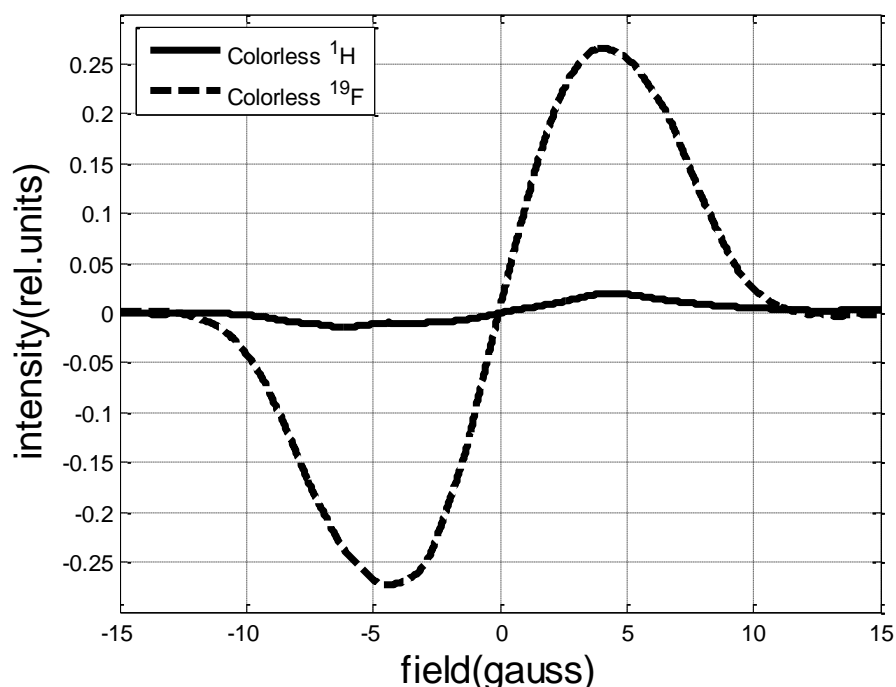


Fig. 1. NMR spectra for  $^1\text{H}$  and  $^{19}\text{F}$  for colorless sample ( $^{19}\text{F}$  more intensive).

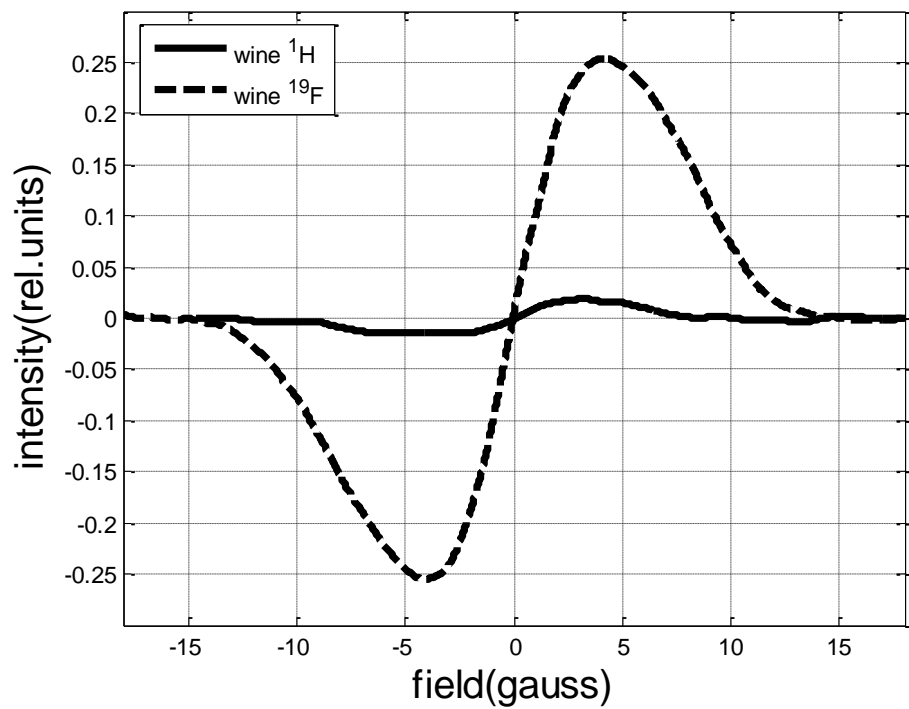


Fig. 2. NMR spectra for <sup>1</sup>H and <sup>19</sup>F for wine sample (<sup>19</sup>F more intensive).

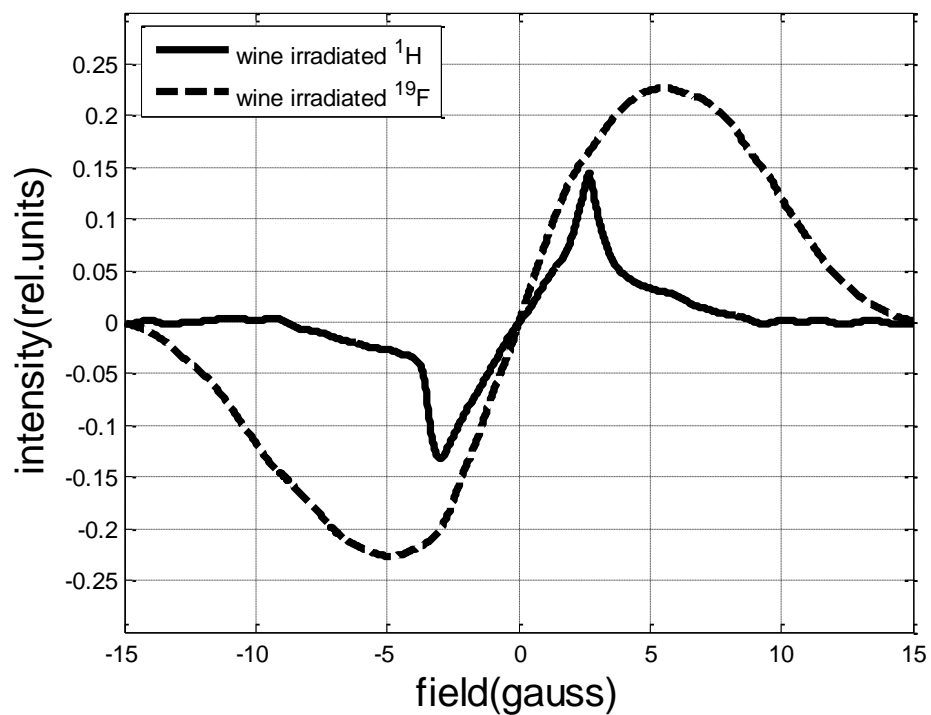


Fig. 3. NMR spectra for <sup>1</sup>H and <sup>19</sup>F for wine irradiated sample(<sup>19</sup>F more intensive).

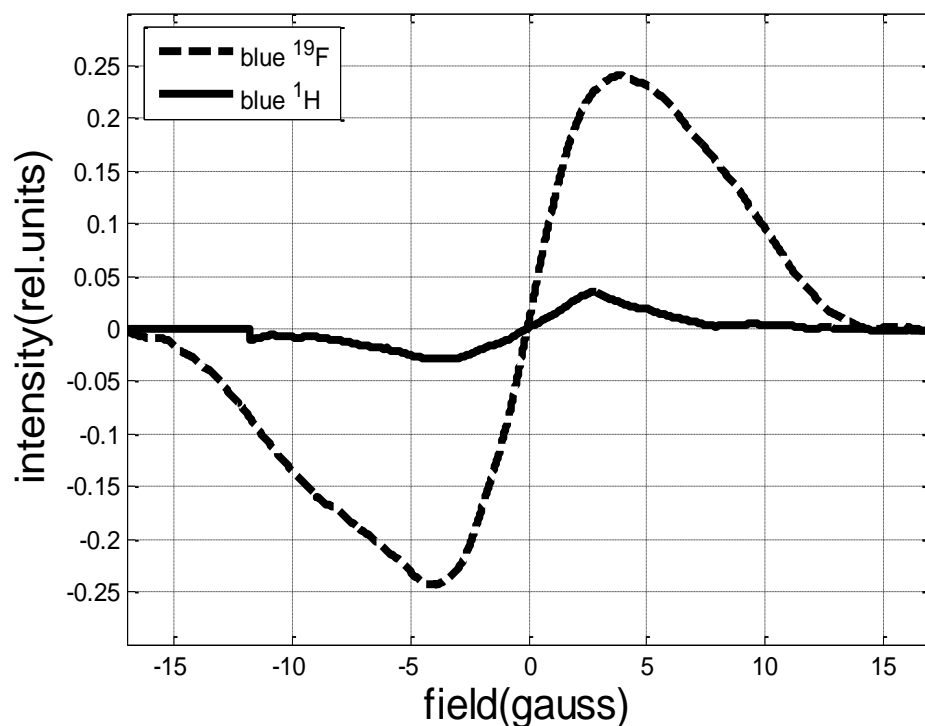


Fig. 4. NMR spectra for  $^1\text{H}$  and  $^{19}\text{F}$  for blue sample.

Relations of integral intensities for each sample are collected in Table 3.

Tabl.3

Integral intensity	H/F
Blue topaz	$0.025 \pm 0.002$
Natural wine topaz	$0.020 \pm 0.002$
Wine irradiated topaz	$0.064 \pm 0.006$
Colorless	$0.014 \pm 0.001$

We can see from the Table that relations of integral intensities of fluorine and hydrogen differ for crystals of different color. In particular, for the wine irradiated topaz this parameter the highest, in comparison with other samples. At the given level of investigations it is too complicated to explain the reason of such difference. It is

possible to assume, that as a result of an irradiation of a wine topaz, structural defects were formed in the crystal lattice of the sample, therefore probably, hydrogen, has taken free positions.

## ***2.2. Experimental definition of the component of electric field gradient tensor***

Also we defined electric field gradients by experiment and ab initio calculations. Ab initio calculations of electric field gradients were based on the functional density method in a pure topaz crystal. For experimental measurement of the component of electric field gradient tensor was used a method of unique rotation.

### **Unique rotation method**

The electric field gradient (EFG) is a symmetric tensor of second rank with zero trace and has only five independent components which are necessary for determination of NMR spectra.

Experimentally we can find the components of the tensor in the random coordinates system, which are defined, as a rule, by a facet of a crystal. Results are represented in the form of main component values of EFG tensor ( $eq$ ), asymmetry parameter ( $\eta$ ) and direction cosine, which is defining direction of the main axes of EFG tensor relative to crystallographic coordinate systems.

The method of unique rotation can be applied only when in a crystal exist crystallographically, but not magnetically, equivalent positions occupied by nuclei from which the NMR spectrum is observed. In the method of unique rotation measurement the orientation dependences is used at crystal rotation around a unique

axis. The direction of a rotation axis should not be perpendicular to the plane of symmetry, reflection in which translates one magnetic-nonequivalent position of a nucleus in another, and there should not be in parallel axes of the symmetry translating one position, occupied with researched nuclei, in another.

Now we consider definition of component electric field gradient tensor. Using as an example a topaz crystal in which there are four magnetic-nonequivalent positions of a nucleus, which transform one in another at reflection in three planes of symmetry. In other words, coordinates of one position transform to coordinates of the second crystallographic position at reflection in symmetry planes which in our case coincide with crystallographic planes. In this case EFG tensor corresponding to these magnetic-nonequivalent positions, in crystallographic to system of coordinates  $a,b,c$ , can be written as follows:

$$\begin{aligned}
 V_{cr}^{(1)} = \begin{pmatrix} V_{aa} & V_{ab} & V_{ac} \\ V_{ab} & V_{bb} & V_{bc} \\ V_{ac} & V_{bc} & V_{cc} \end{pmatrix} &\Leftrightarrow V_{cr}^{(2)} = \begin{pmatrix} V_{aa} & V_{ab} & -V_{ac} \\ V_{ab} & V_{bb} & -V_{bc} \\ -V_{ac} & -V_{bc} & V_{cc} \end{pmatrix} \\
 \Leftrightarrow V_{cr}^{(3)} = \begin{pmatrix} V_{aa} & -V_{ab} & V_{ac} \\ -V_{ab} & V_{bb} & -V_{bc} \\ V_{ac} & -V_{bc} & V_{cc} \end{pmatrix} &\Leftrightarrow V_{cr}^{(4)} = \begin{pmatrix} V_{aa} & -V_{ab} & -V_{ac} \\ -V_{ab} & V_{bb} & V_{bc} \\ -V_{ac} & V_{bc} & V_{cc} \end{pmatrix} \quad (10)
 \end{aligned}$$

Here  $V_{cr}$  is EFG tensors in crystallographic coordinate system corresponding 4 magnetic nonequivalent magnetic positions.

For definition of a component of electric field gradient tensor we rotated the crystal around some axis  $z$ .  $z$ -direction relative to crystallographic systems of coordinates we shall set Euler's corners  $(\delta,\gamma)$  (Fig. 5).  $Y$ -axis of the coordinates system is connected with rotation plane of a crystal in a magnetic field. It is possible to accept a



nonequivalent positions of investigated nucleus: center line and eight first satellites. Center line from nonequivalent site nuclei will join each other if quadrupole coupling is a little. If magnetic field is parallel to a symmetry plane, coinciding with a plane ( $ab$ ), lines in a NMR spectrum will merge in pairs. Last statement becomes obvious if to consider rotation of a crystal around crystallographic  $c$ -axes. In this case in formulas (12) and (13) it is necessary to replace indexes  $x$ ,  $y$ ,  $z$  with indexes  $a$ ,  $b$ ,  $c$  accordingly. Then, as follows from (10)

$$A_c^{(1-4)} = -\frac{1}{2}V_{cc}; B_c^{(1-4)} = \frac{1}{2}(V_{aa} - V_{bb}); C_c^{(1-2)} = -V_{ab}, C_c^{(3-4)} = V_{ab}. \quad (14)$$

Hence, in a NMR spectrum instead of eight satellites lines will be observed only four. Similar situation is observed when rotating around  $a$  and  $b$  axes. At rotation of a crystal around of any  $z$ -axis, at some orientations the magnetic field will be in parallel to one of the crystallographic planes (Fig. 6) and therefore at such orientations the line will merge in to pairs.

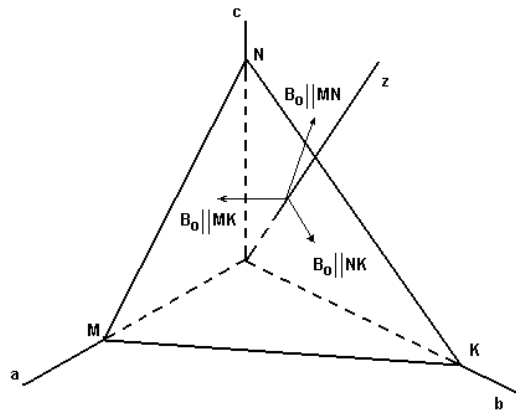
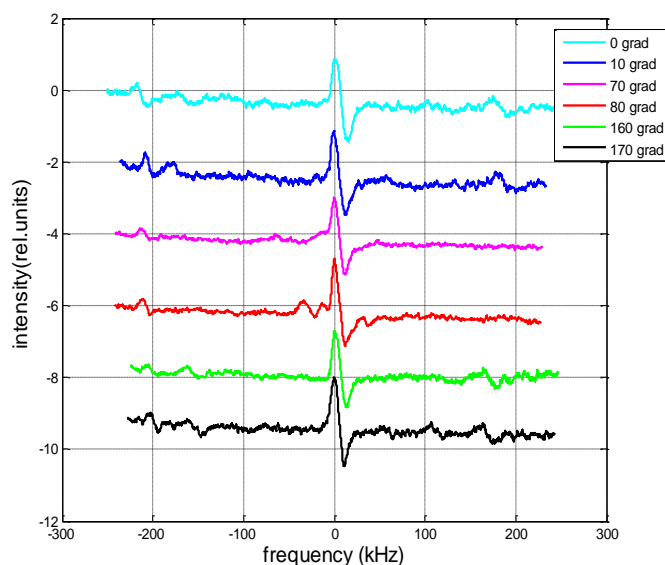


Fig. 6. Scheme of experiment

When we determine the angle  $\phi'$  for such orientations in a magnetic field, we can find angles of a triangle formed by crossing of symmetry plane and plane, which is perpendicular axis of rotation. Knowing these angles, it is easy to find a direction of rotation axis of a crystal in a magnetic field.

Angular dependence of  $^{27}\text{Al}$  NMR spectra has been measured for a monocrystal of a natural blue topaz,  $\text{Al}_2\text{SiO}_4(\text{F}, \text{OH})_2$ . Spectra have been received on a spectrometer of wide lines ПЯ-2301 on frequency of 10.6 MHz. The sample was installed in goniometer to rotate the crystal around the chosen axis, perpendicular to an external magnetic field.

Examples of spectra are resulted in Fig. 7.



*Fig. 7. Examples of NMR spectra on  $^{27}\text{Al}$  when rotating the sample in a magnetic field.*

As far as we can judge from Fig. 7, in a NMR spectrum in a crystal of a blue topaz is observed four satellites corresponding to  $^{27}\text{Al}$  transitions  $m = \pm 3/2 \leftrightarrow \pm 1/2$  and the central line ( $m = 1/2 \leftrightarrow -1/2$ ). Satellite lines are strongly widened because neighboring satellite pairs overlap each other. It means that the direction of rotation axis, which we are choosing, coincides with one of the crystallographic axes. Position of the central peak does not move with rotation of the sample. This allows to make a conclusion that quadrupole interaction is negligible compared to Zeeman interaction. At calculation of NMR spectra it is possible to discard the second order of the perturbation

theory. Intensities of satellite peaks at transition  $m = \pm 5/2 \leftrightarrow \pm 3/2$  practically are not visible on the measured spectra. Therefore, we analyzed only peaks at  $m = \pm 3/2 \leftrightarrow \pm 1/2$  transitions. There is also displaced a line on the spectrum, which shifted relate to the central line  $^{27}\text{Al}$  on 200 KHz. We identified this line, as a line from nucleus  $^{63}\text{Cu}$  in the copper coil in which the sample is placed. To make a conclusion about this line we have record a NMR spectrum for a reference liquid sample containing the liquid aluminium (not hot), placed in the same coil and result has proved to be true.

We divided the lines, overlapped satellites and orientational dependence of shifts of NMR lines. This is represented on Fig. 8.

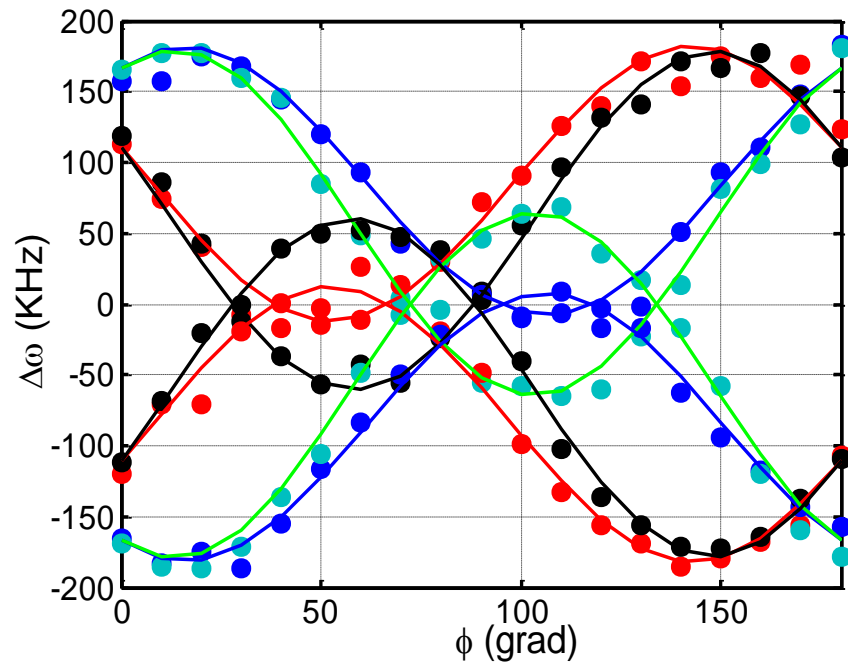


Fig. 8. Orientation dependence of shifts of NMR lines.

From the orientation dependences we find corners of the triangle, forming a plane, perpendicular rotation axes, and then a direction of an rotation axis.

From approximation orientation dependences, we have found values  $A_z^{(1-4)}$ ,  $D_z^{(1-4)}$  and  $\phi_{z0}^{(1-4)}$ , and have calculated sizes

$V_{zz}^{(1-4)}$ ,  $(V_{xx}^{(1-4)} - V_{yy}^{(1-4)})^2 + (V_{xy}^{(1-4)})^2$  and  $V_{xy}^{(1-4)} / (V_{xx}^{(1-4)} - V_{yy}^{(1-4)})$  in the coordinate system connected with rotation of a crystal. Solving system from twelve equations it is possible to find twelve unknown values:  $V_{zz}^{(1-4)}$ ,  $V_{xx}^{(1-4)}$ ,  $V_{xy}^{(1-4)}$  for each of four non-equivalent positions. Next step in the method of unique rotation is transformation of tensors  $V_{cr}^{(1-4)}$  in system of coordinates  $x, y, z$ . Such transformation can be made, if are known direction cosine  $(l, m, n)$  of coordinates system  $x, y, z$  related to crystallographic systems  $(a, b, c)$ :

$$T = \begin{pmatrix} l_1 & l_2 & l_3 \\ m_1 & m_2 & m_3 \\ n_1 & n_2 & n_3 \end{pmatrix}. \quad (15)$$

Then

$$V_{x,y,z}^{(1-4)} = T^{-1} V_{cr} T. \quad (16)$$

Similar to orientation dependences of splitting of the first satellites in coordinate system  $x, y, z$  only three components of the tensor are known:  $V_{zz,xx,xy}^{(1-4)}$ . It is necessary to know, how they are connected with components  $V_{cr}$ . Such ratios for one of positions of a nucleus can be written in form

$$\begin{aligned} V_{zz}^{(1)} &= n_1^2 V_{aa} + n_2^2 V_{bb} + n_3^2 V_{cc} + 2n_1 n_2 V_{ab} + 2n_2 n_3 V_{ac} + 2n_1 n_3 V_{bc}, \\ V_{xx}^{(1)} - V_{yy}^{(1)} &= (l_1^2 - m_1^2) V_{aa} + (l_2^2 - m_2^2) V_{bb} - m_3^2 V_{cc} + 2(l_1 l_2 - m_2 m_1) V_{ab} - 2m_3 m_1 V_{ac} - 2m_2 m_3 V_{bc}, \\ V_{xy}^{(1)} &= l_1 m_1 V_{aa} + l_2 m_2 V_{bb} + (l_2 m_1 + l_1 m_2) V_{ab} + l_1 m_3 V_{ac} + l_2 m_3 V_{bc}. \end{aligned} \quad (17)$$

For the second position these ratio can be write in the form:

$$\begin{aligned} V_{zz}^{(2)} &= n_1^2 V_{aa} + n_2^2 V_{bb} + n_3^2 V_{cc} + 2n_1 n_2 V_{ab} - 2n_2 n_3 V_{ac} - 2n_1 n_3 V_{bc}, \\ V_{xx}^{(2)} - V_{yy}^{(2)} &= (l_1^2 - m_1^2) V_{aa} + (l_2^2 - m_2^2) V_{bb} - m_3^2 V_{cc} + 2(l_1 l_2 - m_2 m_1) V_{ab} + 2m_3 m_1 V_{ac} + 2m_2 m_3 V_{bc}, \\ V_{xy}^{(2)} &= l_1 m_1 V_{aa} + l_2 m_2 V_{bb} + (l_2 m_1 + l_1 m_2) V_{ab} - l_1 m_3 V_{ac} - l_2 m_3 V_{bc}. \end{aligned} \quad (18)$$

Similarly for the third and fourth positions.

Thus, twelve equations to define five unknown constituents of components of EFG tensors in crystallographic system of coordinates are received. After definition of all the components of tensor of a field

gradient, we make diagonalization and also find its main components and a direction of its main axes.

After diagonalization quadrupole interaction constants and asymmetry parameter have been obtained:  $e^2qQ/h = 1.7 \pm 0.1$  MHz,  $\eta = 0.4 \pm 0.1$ . Within the limits of an error, these values coincide with the results received in work [3].

For theoretical calculation we used software package WIEN2k which allows to make not empirical calculations of an electric field gradient, electronic structure of crystals by DFT FLAPW method, density of electronic states, Fermi's level, width of the forbidden zone, etc.

### ***2.3. The density functional theory***

Efficient and accurate method to solve the many-electron problem of a crystal (with nuclei at fixed positions) is the local spin density approximation (LSDA) within density functional theory. Therein the key quantities are the spin densities  $\rho_\sigma(r)$  in terms of which the total energy is

$$E_{tot}(\rho \uparrow, \rho \downarrow) = T_s(\rho \uparrow, \rho \downarrow) + E_{ee}(\rho \uparrow, \rho \downarrow) + E_{Ne}(\rho \uparrow, \rho \downarrow) + E_{xc}(\rho \uparrow, \rho \downarrow) + E_{NN} \quad (19)$$

where  $E_{NN}$  is the repulsive Coulomb energy of the fixed nuclei and the electronic contributions, labeled conventionally as, respectively,  $T_s(\rho \uparrow, \rho \downarrow)$  is kinetic energy (of the non-interacting particles),  $E_{ee}(\rho \uparrow, \rho \downarrow)$  is electron-electron repulsion,  $E_{Ne}(\rho \uparrow, \rho \downarrow)$  is nuclear-electron attraction, and  $E_{xc}(\rho \uparrow, \rho \downarrow)$  is exchange-correlation energies. Two approximations comprise the LSDA, i), the assumption that  $E_{xc}$  can be written in terms of a local exchange-correlation energy density  $\mu_{xc}$  times the total (spin-up plus spin-down) electron density as

$$E_{xc} = \int \mu_{xc}(\rho \uparrow, \rho \downarrow) * [\rho \uparrow + \rho \downarrow] dr \quad (20)$$

and ii), the particular form chosen for that  $\mu_{xc}$ .  $E_{tot}$  has a variational equivalence with the familiar Rayleigh-Ritz principle. The most effective way known to minimize  $E_{tot}$  by means of the variational principle is to introduce orbitals  $ik$  constrained to construct the spin densities as

$$\rho_{\sigma}(r) = \sum_{i,k} \rho_{ik}^{\sigma} |\chi_{ik}^{\sigma}(r)|^2. \quad (21)$$

Here, the  $\rho_{ik}^{\sigma}$  are occupation numbers such that  $0 \leq \rho_{ik}^{\sigma} \leq 1/\omega_k$ , where  $\omega_k$  is the symmetry-required weight of point  $k$ . Then variation of  $E_{tot}$  gives the Kohn-Sham equations (in Ry atomic units),

$$[-\nabla^2 + V_{Ne} + V_{ee} + V_{xc}^{\sigma}] \chi_{ik}^{\sigma}(r) = \epsilon_{ik}^{\sigma} \chi_{ik}^{\sigma}(r), \quad (22)$$

which must be solved and thus constitute the primary computational task. This Kohn-Sham equations must be solved self-consistently in an iterative way, since finding the Kohn-Sham orbitals requires information of the potentials which themselves depend on the (spin-) density and thus on the orbitals again. Recently exist progress going beyond the LSDA by adding gradient terms of the electron density to the exchange-correlation energy or its corresponding potential. This has led to the generalized gradient approximation (GGA) with various parameterizations. A recent version the evaluation of the exchange-correlation energy not only the gradient of the density, but also the kinetic energy density  $\tau(r)$ . Unfortunately, such schemes are not yet self-consistent.

## Full Potential Augmented Plane Wave Methods

The linearized augmented plane wave (LAPW) method is among the most accurate methods to perform electronic structure calculations for crystals. It is based on the density functional theory for the treatment of exchange and correlation and uses e.g. LSDA. Several forms of LSDA potentials exist in the literature, but recent improvements use the generalized gradient approximation (GGA) are available too. For valence states relativistic effects can be included either in a scalar relativistic treatment or with the second variational method including spin-orbit coupling. Like most “energy-band methods“, the LAPW method is a procedure for solving the Kohn-Sham equations for the ground state density, total energy, and (Kohn-Sham) eigenvalues (energy bands) of a many-electron system (here a crystal) by introducing a basic set which is especially adapted to the problem.

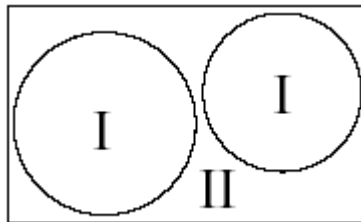


Fig. 9: Partitioning of the unit cell into atomic spheres (I) and an interstitial region (II).

In this adaptation the unit cell is divided into (I) non-overlapping atomic spheres (centered at the atomic sites) and (II) an interstitial region. In two types of regions following different basic sets are used:

## *The APW Methods.*

**1. Inside atomic sphere  $t$  (I), of radius  $R_t$ ,** a linear combination of radial functions times spherical harmonics  $Y_{lm}(r)$  is used (we omit the index  $t$  when it is clear from the context)

$$\Phi_{\vec{k}_n} = \sum_{lm} [A_{lm}(r)u_l(r, E_l) + B_{lm}\dot{u}_l(r, E_l)]Y_{lm}(\theta, \varphi), \quad (23)$$

where  $U_l(r, E_l)$  is the regular solution (at the origin) of the radial Schrodinger equation for energy  $E_l$  (chosen normally at the center of the corresponding band with  $l$ -like character) and the spherical part of the potential inside sphere  $t$ ;  $\dot{U}_l(r, E_l)$  is the time derivative of  $U_l$  evaluated at the same energy  $E_l$ . A linear combination of these two functions constitute the linearization of the radial function; the coefficients  $A_{lm}$  and  $B_{lm}$  are functions of  $k_n$  (see below).  $A_{lm}$  and  $B_{lm}$  determined by requiring that this basis function matches (in value and slope) each plane wave (PW)  $U_l$  and  $\dot{U}_l$  are obtained by numerical integration of the radial Schrödinger equation on a radial mesh inside the sphere.

**2. In the interstitial region (II)** a plane wave expansion is used

$$\Phi_{\vec{k}_n} = \frac{1}{\Omega} e^{i\vec{k}_n \vec{r}}, \quad (24)$$

where  $\vec{k}_n = \vec{k} + \vec{K}_n$ ,  $\vec{K}_n$  are the reciprocal lattice vectors and  $\vec{k}$  is the wave vector inside the first Brillouin zone. Each plane wave is augmented by an atomic-like function in every atomic sphere.

The solutions of the Kohn-Sham equations are expanded in this combined basis set of LAPW's according to the linear variation method

$$\psi_{\vec{k}} = \sum_n C_n \Phi_{\vec{k}_n}. \quad (25)$$

Here the coefficients  $C_n$  are determined by the Rayleigh-Ritz variational principle. The convergence of this basis set is controlled by a cutoff parameter  $R_m K_{\max} = 6-9$ , where  $R_m$  is the smallest atomic sphere radius in the unit cell and  $K_{\max}$  is the magnitude of the largest  $K$  vector in equation (25). In order to improve the linearization, i.e. to increase the flexibility of the basic and to make possible a consistent treatment of semicore and valence states in one energy window additional  $kn$  independent basic functions can be added. They are called “local orbitals (LO)” [33] and consist of a linear combination of 2 radial functions at 2 different energies, e.g. at the 3s and 4s energy, and one energy derivative at one of these energies:

$$\Phi_{lm}^{LO} = [A_{lm}u_l(r, E_{1,l}) + B_{lm}\dot{u}_l(r, E_{1,l}) + C_{lm}u_l(r, E_{2,l})]Y_{lm}(\hat{r}). \quad (26)$$

The coefficients  $A_{lm}$ ,  $B_{lm}$  and  $C_{lm}$  can be determined by the requirements that  $\phi^{LO}$  should be normalized and has zero value and slope at the sphere boundary.

### **The APW+lo method**

Sjostedt, Nordstrom and Singh [34] have shown that the standard LAPW method with additional constraint on the PWs of matching in value and slope to the solution inside the sphere is not the most efficient way to linearize Slater’s APW method. It can be made much more efficient when one uses the standard APW basis, but of course with  $u_l(r, E_l)$  at a fixed energy  $E_l$  in order to keep the eigenvalue problem linear. One then adds a new local orbital (*lo*) to have enough variational flexibility in the radial basis functions:

$$\Phi_{\bar{k}_n} = \sum_{lm} [A_{lm,k_n} u_l(r, E_l)] Y_{lm}(r). \quad (27)$$

$$\Phi_{lm}^{lo} = [A_{lm} u_l(r, E_{1,l}) + B_{lm} \dot{u}_l(r, E_{1,l})] Y_{lm}(\hat{r}). \quad (28)$$

This new lo (denoted with lower case to distinguish it from the LO given in Eq. 26) looks almost like the old ‘‘LAPW’’-basis set, but here the  $A_{lm}$  and  $B_{lm}$  do not depend on  $k_n$  and are determined by the requirement that the lo is zero at the sphere boundary and normalized. Thus we construct basis functions that have ‘‘kinks’’ at the sphere boundary, which makes it necessary to include surface terms in the kinetic energy part of the Hamiltonian. Note, however, that the total wave-function is of course smooth and differentiable. As shown by Madsen et al. [35] this new scheme converges practically to identical results as the LAPW method, but allows to reduce ‘‘ $RK_{\max}$ ’’ by about one, leading to significantly smaller basic sets (up to 50 %) and thus the corresponding computational time is drastically reduced (by an order of magnitude). Within one calculation a mixed ‘‘LAPW and APW+lo’’ basis can be used for different atoms and even different  $l$ -values for the same atom (Madsen et al. 2001). In general, one describes by APW+lo those orbitals which converge most slowly with the number of PWs (such as TM 3d states) or the atoms with a small sphere size, but the rest with ordinary LAPWs. One can also add a second LO at a different energy so that both, semicore and valence states, can be described simultaneously.

By this program the electric fields gradient has been calculated, the constant of quadrupole interaction (1.50 MHz) and parameter of asymmetry 0.86 is received. The experimental and calculated values of electric fields gradient tensors differ from each other. The reason is, apparently, that in calculations we used the ideal structure of a topaz which are does not contain any impurity and hydroxyl groups. The

constant of quadrupole interaction and  $eq_{zz}$  – component of EFG are proportional to each other.

For the analysis of separate contributions of electric fields gradient we have calculated density of electronic states, dependence of size tensor a of electric fields gradient (EFG) from radius of sphere inside of which are located electrons, considered at calculation of tensor EFG (Fig. 10).

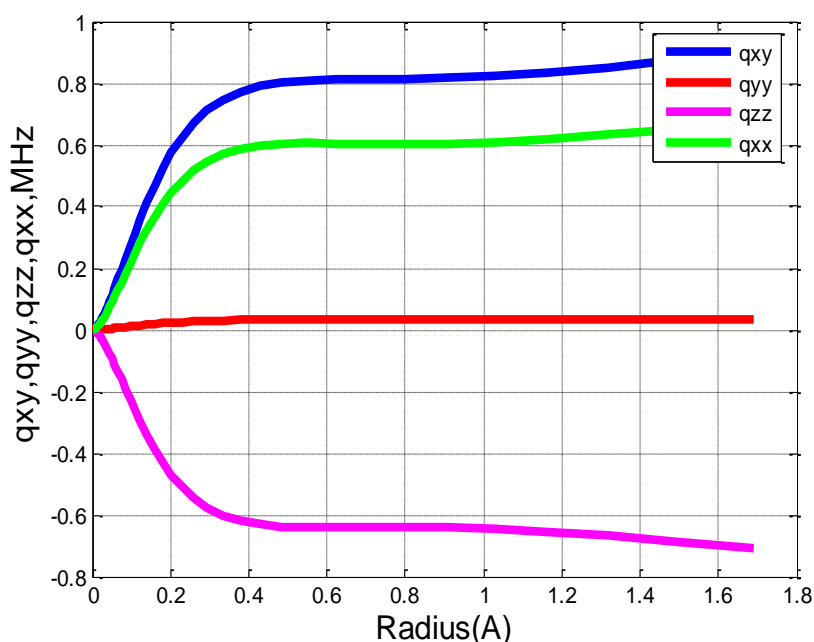


*Fig. 10. Dependence of size tensor of EFG from radius of sphere inside of which are located electrons. The values  $q_{zz}$ ,  $q_{xx}$ , and  $q_{yy}$  are defined in crystallographic system coordinates.*

As we can see from figure the basic contribution from tensor EFG are defined electrons, located inside of sphere with radius 0.4 A.

In Figs. 11 - 15 (we have calculated density of electronic states) electronic density distribution on energy levels is presented:

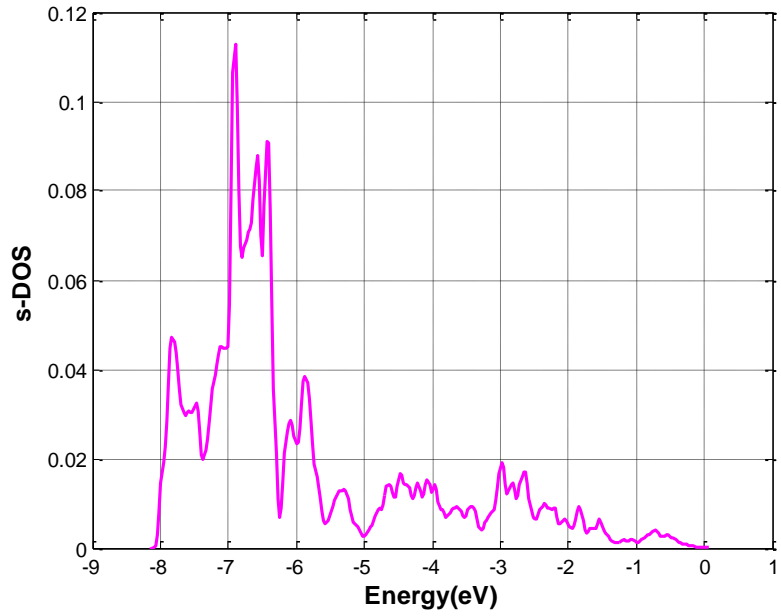


*Fig. 11. The contribution of s-electrons in the general electronic density.*

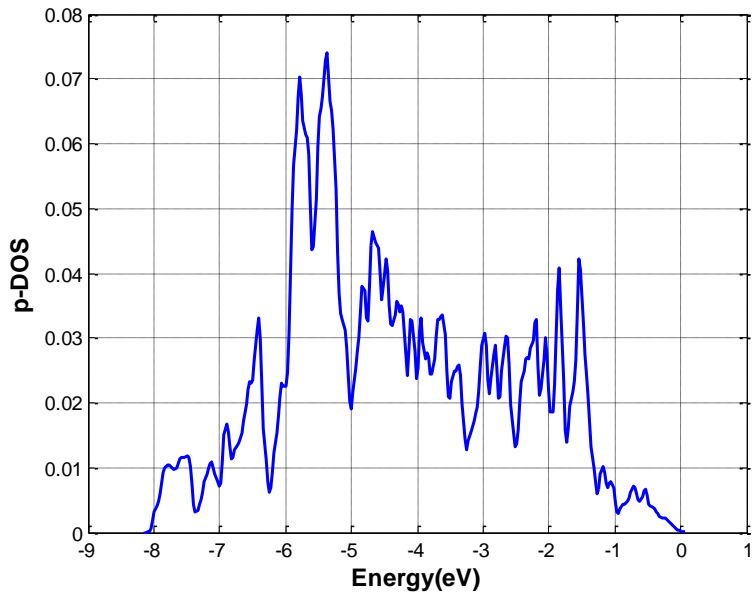


*Fig. 12. The contribution of p-electrons in the general electronic density.*

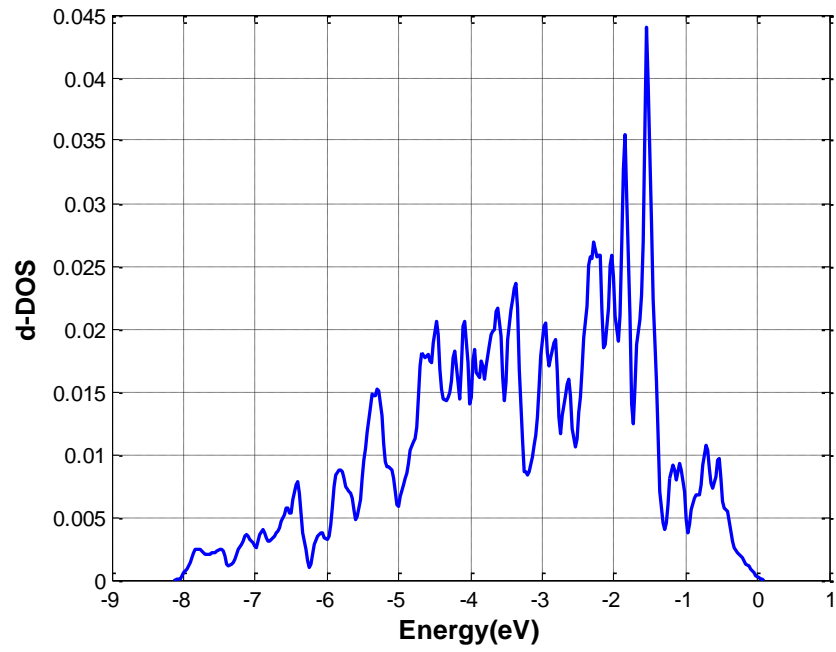


*Fig. 13. The contribution d-electrons in the general electronic density.*

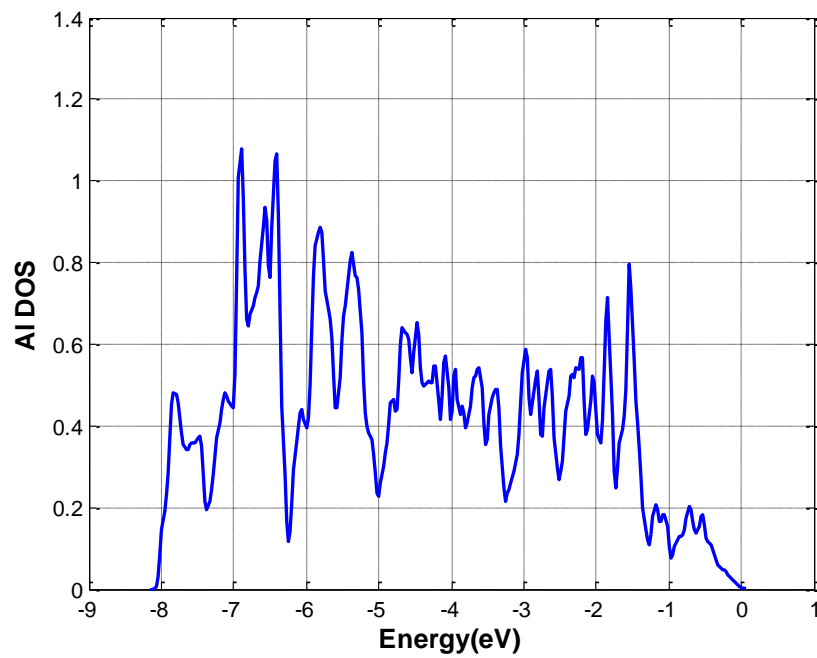


*Fig. 14. The contribution of electrons in the aluminium atom in the general electronic density.*

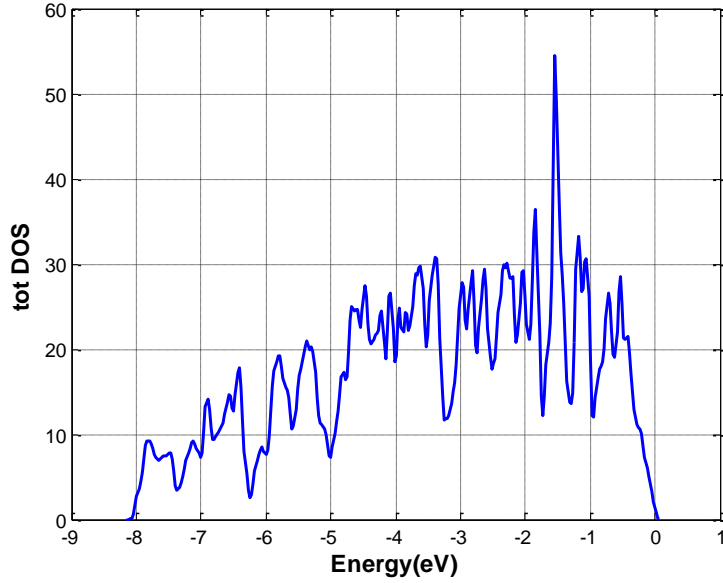


*Fig. 15. The contribution of all electrons of crystal in the general electronic density.*

As we can see from figures, the electron contribution of all aluminium atoms which are exist in the unit cell in full value of electronic density of state (DOS) is much less than electrons contribution from other atoms. A qualitative analysis of contributions of separate electronic shell in the EFG tensor can be made from the calculated electronic density of states. The main contribution of electronic density in the EFG tensor in atom of aluminium is the contribution from electrons with energy close to Fermi level. Therefore it is possible to assume, that EFG tensor is determined p-electrons, since value of gradients of an electric field inversely proportional  $L^3$ , where  $L$  - the orbital moment of a corresponding shell.

For quantitative analysis of contributions of separate environments in EFG tensor, we have calculated these contributions using package Wien2k. Total EFG tensor has following values in MHz in crystallographic coordinate system:

$$V = \begin{pmatrix} 0.67378 & 0.91803 & 0.02621 \\ 0.91803 & 0.03509 & -0.97305 \\ 0.02621 & -0.97305 & -0.70887 \end{pmatrix}$$

Types of tensors on all *sd*, *pp*, *dd*-electrons:

$$V_{pp} = \begin{pmatrix} 0.64566 & 0.85214 & -0.00976 \\ 0.85214 & 0.03512 & -0.96601 \\ -0.00976 & -0.96601 & -0.68041 \end{pmatrix}$$

$$V_{sd} = \begin{pmatrix} 0.00636 & 0.00955 & 0.00214 \\ 0.00955 & 0.00031 & -0.00411 \\ 0.00214 & -0.00411 & -0.00666 \end{pmatrix}$$

$$V_{dd} = \begin{pmatrix} 0.00772 & 0.02717 & 0.01931 \\ 0.02717 & -0.00071 & -0.00575 \\ 0.01931 & -0.00575 & -0.00700 \end{pmatrix}.$$

Thus calculations confirm the conclusion which was made from the analysis of electronic density of state on energy levels: p-electrons give the basic contribution in EFG tensor.

### 3. SPIN-LATTICE RELAXATION TIME

#### 3.1. Theoretical background.

Natural minerals usually contain a considerable amount of paramagnetic impurities which might produce structural disorders. Those impurities act as relaxation centers for nuclear spins [28].

*Spin-lattice relaxation time*, known as  $T_1$ , characterizes the rate at which the longitudinal component of the magnetization vector,  $M_z$ , recovers:

$$M_z(t) = M_0 e^{-t/T_1} \quad (29)$$

$M_0$  it is equilibrium value of the magnetization.

The relaxation time,  $T_1$ , the average lifetime of nuclei in the higher energy state is dependent on the mobility of the nuclei in the lattice. As mobility increases, the vibrational and rotational frequencies increase, making it more likely for a lattice field component to be able to interact with excited nuclei. However, at extremely high mobilities, the probability of a lattice field component to interact with excited nuclei decreases. The relaxation times for the same nuclei in different lattice sites can vary in wide range. The rate of relaxation time strongly depends on the relaxation mechanisms (see Table 4)

Tabl.4

Interaction	Range of interaction (Hz)	relevant parameters
1-Dipolar coupling	$10^4 - 10^5$	-abundance of magnetically active nuclei - size of the magnetogyric ratio

2-Quadrupolar coupling	$10^6 - 10^9$	- size of quadrupolar coupling constant - electric field gradient at the nucleus
3- Paramagnetic	$10^7 - 10^8$	concentration of paramagnetic impurities
4- Scalar coupling	$10 - 10^3$	size of the scalar coupling constants
5-Chemical Shift Anisotropy (CSA)	$10 - 10^4$	- size of the chemical shift anisotropy - symmetry at the nuclear site

Bloembergen first performed a serie of experiments which outlined the main features of the paramagnetic relaxation mechanism. In brief, the dipolar interaction between the moment of paramagnetic ion and the nuclear moment gives for the nuclear spin a transition probability proportional to  $r^{-6}$ , where  $r$  is the distance between paramagnetic ion and nucleus. Therefore nuclear spins lying close to the impurity are rapidly relaxing. Nuclear spins far from the impurity ion do not «feel» this direct dipolar interaction. Nevertheless, by exchange of energy through mutual flips with neighboring nuclei via the nuclear dipole-dipole interaction, nuclear magnetization can travel by a random walk process through the crystal toward the impurity ion. The bulk nuclear magnetization thus relaxes toward its equilibrium value in accordance with the “spin-diffusion” equation,

$$\frac{\partial M}{\partial t} = D\nabla^2 M - C(M - M_0) \sum_n |r - r_n|^{-6}. \quad (30)$$

In this equation,  $D$  represents the spin diffusion coefficient,  $C$  the strength of the dipole-dipole interaction between paramagnetic ion moment and nuclear moment, and  $M_0$  the equilibrium value of the

nuclear magnetization [29]. The diffusion equation has been solved independently by de Gennes and by Khutsishvili [30], making use of boundary conditions applicable to dilute paramagnetic impurities. Their solution predicts that the magnetization relaxes exponentially toward its equilibrium value  $M_0$  with a time constant given by  $1/T_1 \sim N_0$  where  $N_0$  is the number of paramagnetic ions per cubic centimeter.

When  $I = 1/2$ , nuclear relaxation proceeds according to the solutions of de Gennes, Khutsishvili and Bloembergen. For spin  $I > 1/2$ , a description of the relaxation process can be obtained from solutions of the master rate equations for the populations of the master rate equations of the  $(2I+1)$  energy levels. In particular, interest is centered to the case of equally spaced energy levels and to the case of unequally spaced energy levels. In the former case, one would expect that the concept of local spin temperature would be applicable. In this case the recovery of the total magnetization may be shown to follow a single exponential dependence, characteristic of the constants  $C$  and  $D$  when suitably modified by their dependence on  $I$ . In the second case, the magnetization recovery of an adjacent pair of levels is described by a linear combination of  $(2I)$  exponential functions whose individual characteristic times are related to  $C$  and  $D$  [29]. First, in the limiting case of equally spaced energy levels, these solutions reduce to a single exponential term; a unique spin-lattice relaxation time  $T_1$  can be defined. Second, even for unequally spaced levels, any pair of level populations recovers asymptotically to thermal equilibrium as an exponential with this same time constant  $T_1$  [29].

In a crystal at finite temperature, lattice vibrations produce a fluctuating crystalline electric field, which in turn perturbs the orbital motion of the outer paramagnetic ion electrons [29].

## **3.2. Experimental part**

### **3.2.1. Sample preparation**

In experiment were used 4 types of topazes from Volhynia, Ukraine: 2 natural crystals (colorless and blue) and 2 irradiated samples of blue color with different color intensity with names sky blue and Swiss blue. Swiss blue sample has more intensive blue color. Further, topazes were crushed in a powder up to fraction of 0.2 - 0.3 mm. Measurements were done on powders at room temperature. Then, powders were heated up to temperatures: 150 °C, 180 °C, 200 °C, 250 °C, 300 °C, 400 °C and 500 °C. Each sample was kept in the furnace at each temperature for 3 hours, cooled during 12 hours and then measured at room temperature after cooling.

### **3.2.2. The measurements**

Nuclear spin-lattice relaxation of  $^{27}\text{Al}$  in the topaz powders with different colors (natural blue, colorless, sky blue irradiated and Swiss blue irradiated) were investigated (150 °C, 180 °C, 200 °C, 220 °C, 250 °C, 300 °C, 400 °C, 500 °C) by NMR method. NMR measurements were made by using a Bruker Avance DSX 300. The resonance frequency for  $^{27}\text{Al}$  was set at 78.2 MHz. The inversion recovery pulse sequence  $[\pi\text{-}t\text{-}\pi/2]$  was used in order to measure the spin-lattice relaxation time  $T_1$ . We measured the  $T_1$  values of  $^{27}\text{Al}$  by exciting only the central line resonance. All relaxation curves for 4 different samples are shown on Fig. 16.

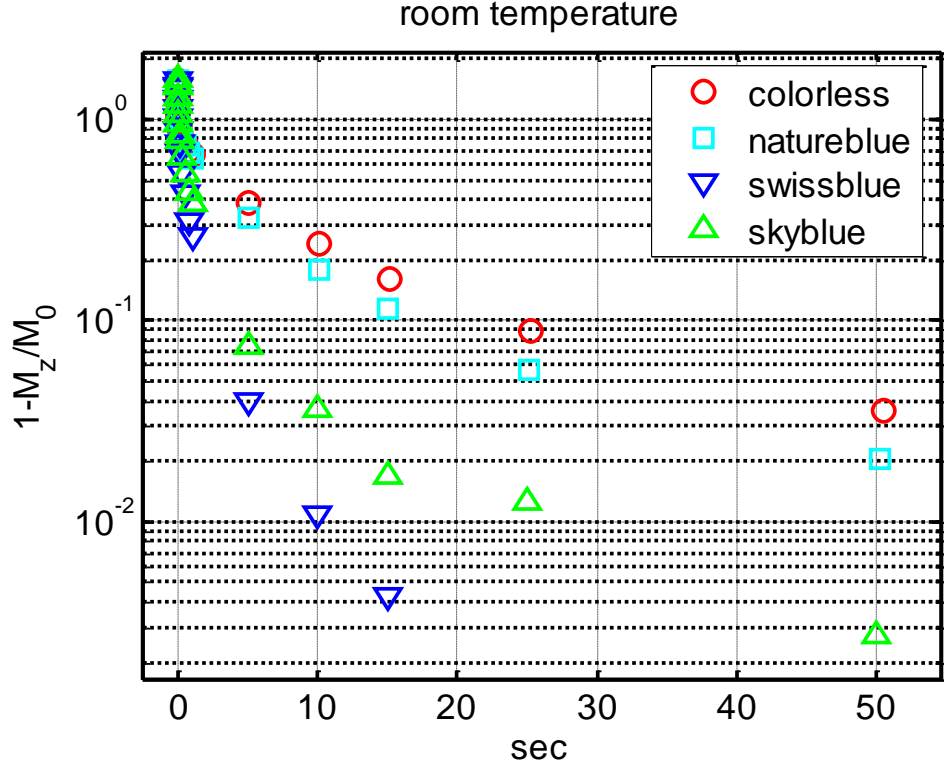


*Fig. 16. Relaxation curves for 4 different topaz powders with different colors at room temperature.*

The spin-lattice relaxation is well described by the linear combination of three exponential functions:

$$\frac{M(\infty) - M(t)}{M(\infty)} = C_1 \exp\left(\frac{-2t}{T_1}\right) + C_2 \exp\left(\frac{-6t}{T_1}\right) + C_3 \exp\left(\frac{-15t}{T_1}\right) + C_4 \exp\left(\frac{-t}{T_1'}\right) \quad (31)$$

We choose the coefficients  $C_i$  of exponent function to well describe the magnetization behavior. Coefficients depend on a condition of longitudinal magnetization after  $180^\circ$  impulses. In our case there was no full inversion of magnetization, therefore we choose this one manually. The  $C_i$  were chosen to describe behaviour of a relaxation time in the best way. The initial condition was similar for each powdered samples, therefore also coefficients were equal in the limit of error.

The contributions of quadrupole mechanism to the spin-lattice relaxation are negligible compared with the paramagnetic one. The relaxation times were different for each sample: at room temperature for colorless sample  $11.5 \pm 1$  s, for natural blue sample  $8.5 \pm 1$  s, for Swiss blue irradiated sample  $1.1 \pm 0.5$  s and for sky blue irradiated sample  $2.1 \pm 0.5$  s. It means that in irradiated samples there are a little bit more paramagnetic impurities.

Relaxation curves for each kind of samples at different temperatures are presence on Fig. 17 - 20.

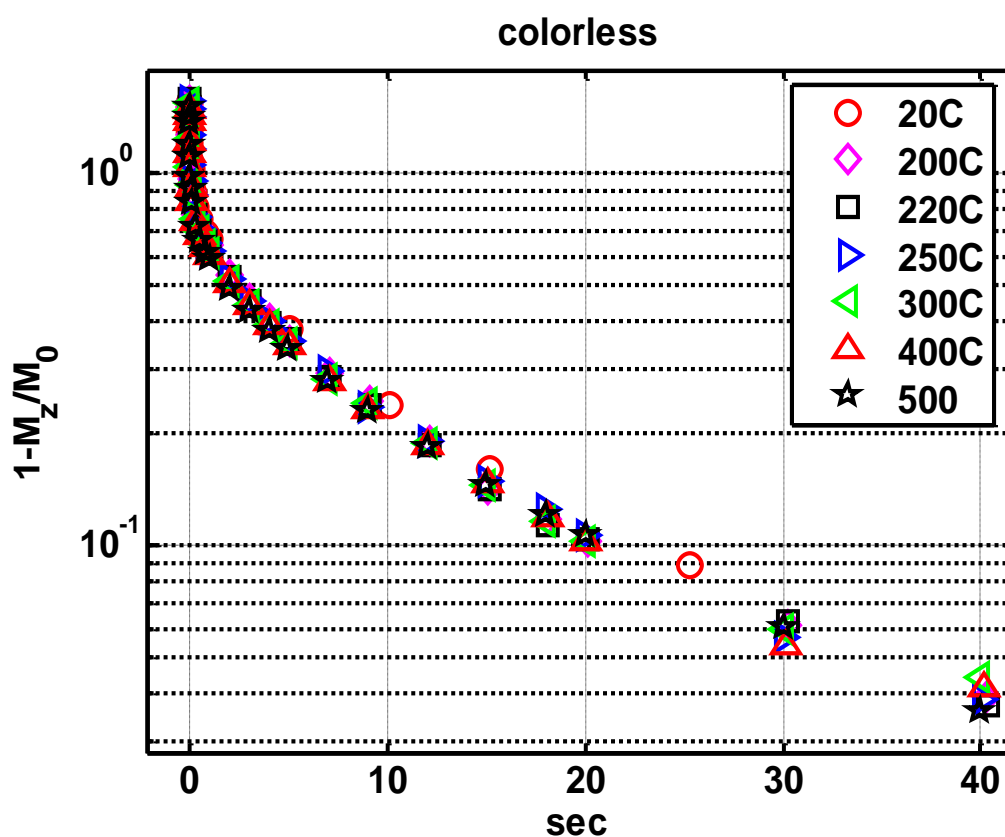


Fig. 17. Relaxation curves for powdered colorless topaz after heated at different temperatures.

As we can see from the figure for powdered colorless topaz, no some changes in relaxation time values within the limit of error. It is possible to correlate with environmental conditions, in which the crystal was formed, there are no additional influence, such as radiation.

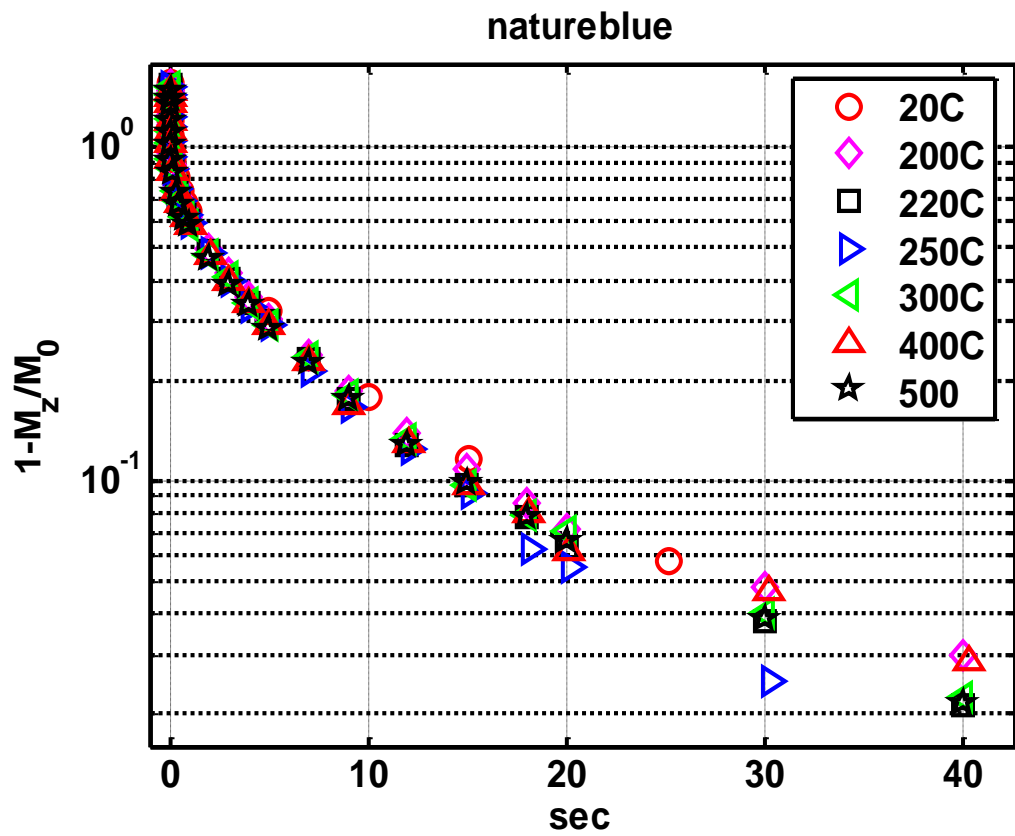


Fig. 18. Relaxation curves for powdered natural blue topaz after heated at different temperatures.

As we can see from the figure for powdered natural blue topaz, no some changes in relaxation time values in the limit of error.

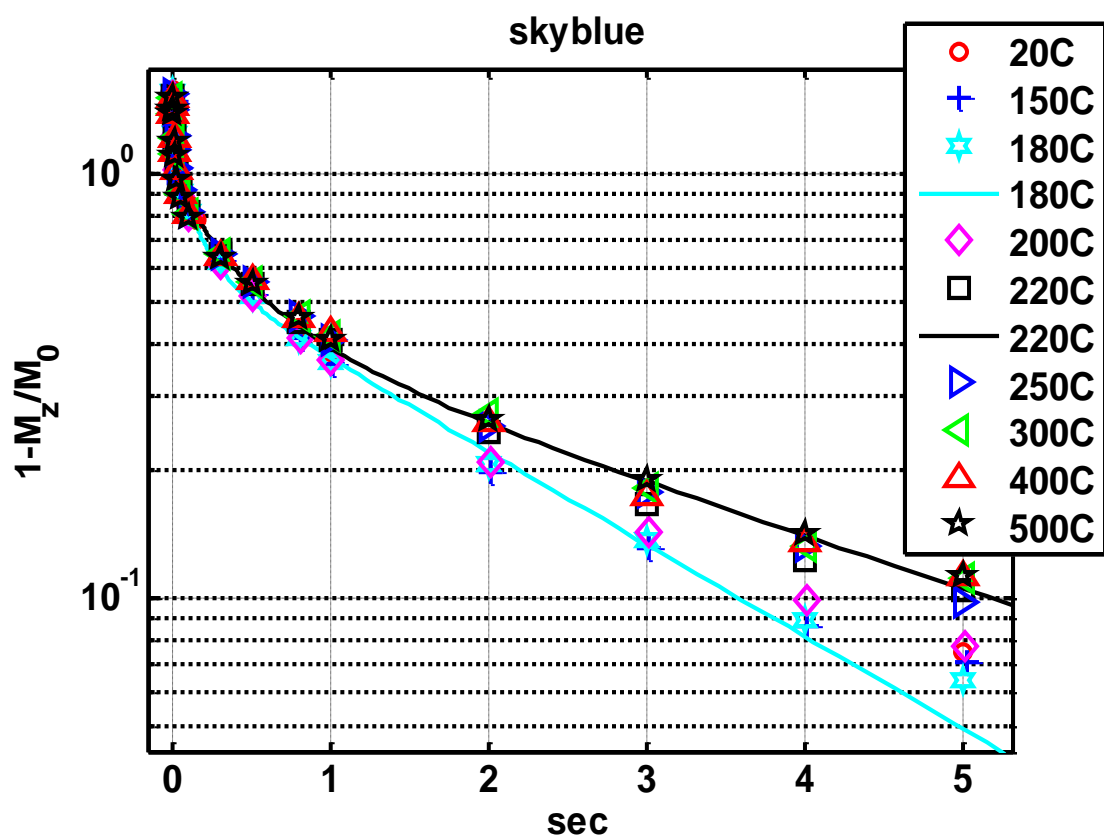


Fig. 19. Relaxation curves for powdered sky blue irradiated topaz after heated at different temperatures.

For sky blue irradiated topaz changes in relaxation time values were observable. In temperature below 200 °C no changes, but at temperature 220 °C there was increasing of relaxation time value, which remains constant until 500 °C. It was possible to correlate with paramagnetic centers, which were destroyed by temperature influence. At 220 °C it is possible to see small changing of topaz color.

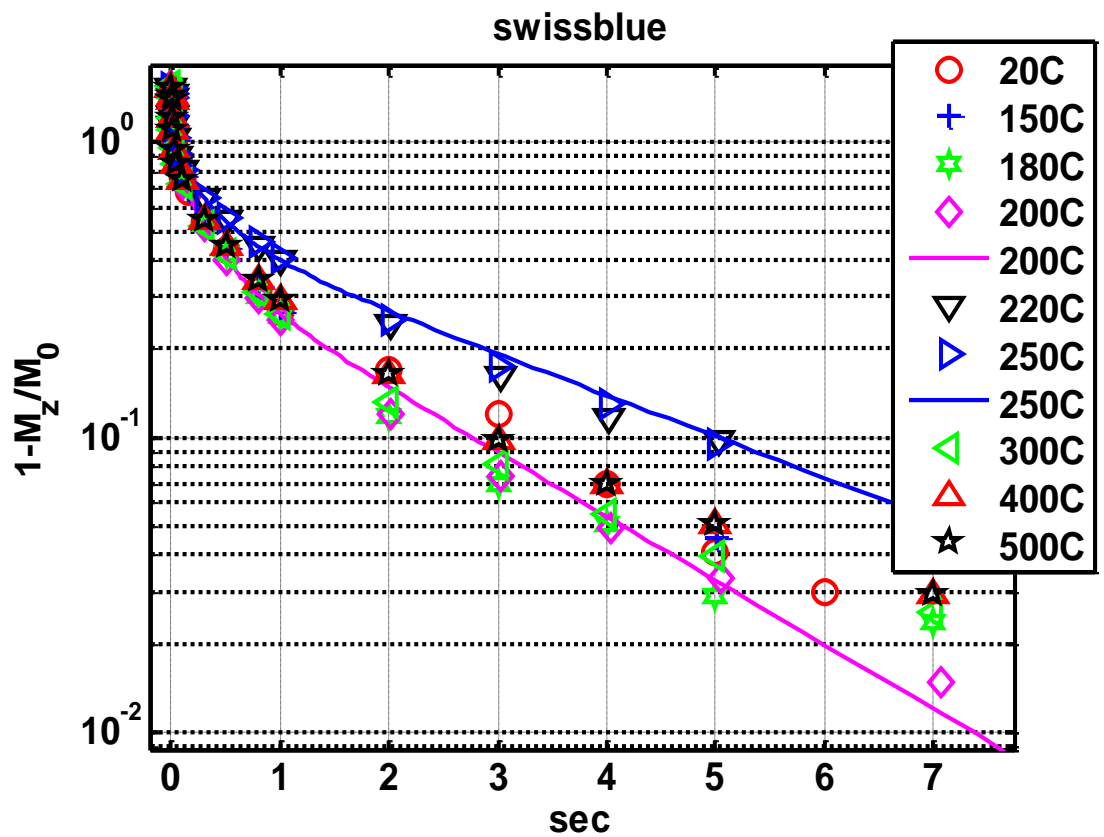


Fig. 20. Relaxation curves for powdered Swiss blue irradiated topaz after burned at different temperatures. Lines are approximation by three exponential functions.

For Swiss blue irradiated topaz also there are some changes in relaxation time values. Below 200 °C no changes, but at 220 – 250 °C relaxation time increases, and at 300 – 500 °C again  $T_1$  decreases.

Magnetization recovery as a result of approximation is present on Fig. 21.

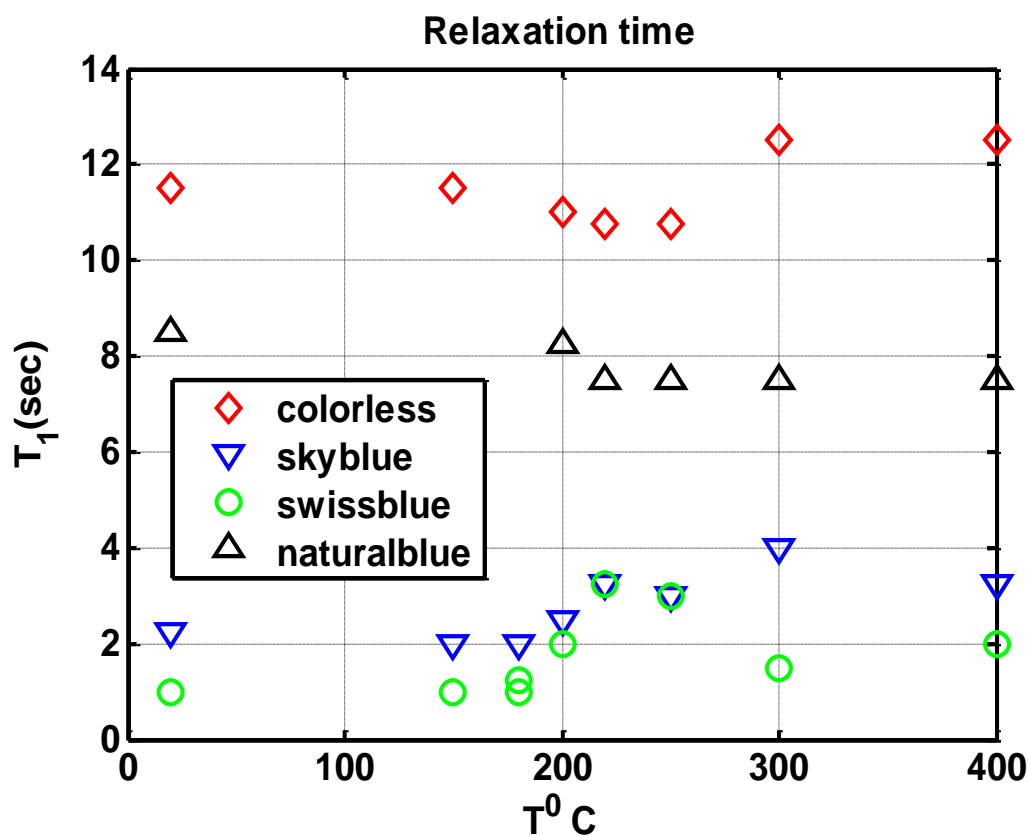


Fig. 21. Temperature dependence of the relaxation time.

As we can see from the figure, spin-lattice relaxation time for irradiated samples changes in temperature range 200 – 250 °C. Exactly in this interval also topazes colors changes. For natural powdered topazes (without irradiation)  $T_1$  change is very negligible compare to irradiated samples. It is possible to correlate with amount of paramagnetic impurities and structural disorders.

## CONCLUSIONS

The largest value for F/OH relation was observed for the wine irradiated crystal of a topaz, and the smallest for colorless one. It can be correlated with relaxation time values, which are determined by the amount of the paramagnetic centers.

We measured the constant of quadrupole coupling and parameter of asymmetry for natural blue sample. These values ( $e^2qQ/h = 1.7 \pm 0.1$  MHz,  $\eta = 0.4 \pm 0.1$ ) coincide with the results received in work [32] within the limits of an error. The directions of principal axes of the EFG tensor of  $^{27}\text{Al}$  were near to the directions of Al – O and Al – F bonds.

We calculated EFG for ideal structure of a topaz by FLAPW method. The calculated value of a quadrupol coupling constant ( $e^2qQ/h = 1.50$  MHz) is very close to experimentally received value ( $e^2qQ/h = 1.7 \pm 0.1$  MHz), whereas the asymmetry parameter differs almost twice (calculated value  $\eta = 0,86$  and experimental value  $\eta = 0.4$ ). This difference can be explained by presence of paramagnetic impurity and OH groups.

For the analysis of separate EFG contributions we have calculated density of electronic states, dependence of EFG tensor from radius of sphere inside of which electrons are located. The analysis of density of electronic conditions and calculation of contributions of separate electronic environments in EFG tensor show, that the basic contribution in EFG tensor is given by p-electrons, and by electrons located inside of sphere of radius  $0.4 \text{ \AA}$ .

The measured relaxation times dependences on heating temperature of samples showed that colorless sample contain smallest

amount of the paramagnetic centers; the blue topaz contains larger amount of impurities. For natural samples the amount of the paramagnetic centers remain constant up to 500 °C. For the irradiated samples the amount of the paramagnetic centers changes when temperature change in a range 200 – 250 °C.

## REFERENCES

- [1] M. V. B. Pinheiro, C. Fantini, K. Krambrock, A. I. C. Persiano, M. S. S. Dantas, and M. A. Pimenta, OH/F substitution in topaz studied by Raman spectroscopy *Physical Review B*, v. 65, 104301, 2002.
- [2] Divaniözia N. Souza, Mario Ernesto G. Valerio, Jose Fernandes de Lima, Linda V.E. Caldas, Dosimetric properties of natural brazilian topaz: A thermally stimulated exoelectronic emission and thermoluminescence study, *Nuclear Instruments and Methods in Physics Research B* 166±167 (2000) 209-214
- [3] Xianyu Xue, Masami Kanzaki, Hiroshi Fukui, Eiji Ito, Takafumi Hashimoto “Cation order and hydrogen bonding of high-pressure phases in the Al<sub>2</sub>O<sub>3</sub>-SiO<sub>2</sub>-H<sub>2</sub>O system” Abstract for oral presentation at Annual Meeting for the Mineralogical Society of Japan, Sept. 21-23, Matsuyama, Ehime, Japan
- [4] Pichavant M, Manning D (1984) Petrogenesis of tourmaline granites and topaz granites: the contribution of experimental data. *Phys Earth Plan Int* 35:31–50
- [5] Taylor RP, Fallick AE (1997) The evolution of fluorine-rich felsic magmas: source dichotomy, magmatic convergence and the origins of topaz granite. *Terra Nova* 9:105–108
- [6] Zhang RY, Liou JG, Shu JF (2002) Hydroxyl-rich topaz in high pressure and ultrahigh-pressure kyanite quartzites, with retrograde woodhouseite, from the Sulu terrane, eastern China. *Am Mineral* 87:445–453
- [7] Alberico A, Ferrando S, Ivaldi G, Ferraris G (2003) X-ray singlecrystal structure refinement of an OH-rich topaz from Sulu UHP terrane (Eastern China)—structural foundation of the correlation between cell parameters and fluorine content. *Eur J Mineral* 15:875–881
- [8] Alston NA, West J (1928) The structure of topaz. *Proc R Soc A* 121:358–367
- [9] Pauling L (1928) The crystal structure of topaz. *Proc Natl Acad Sci USA* 14:603–606
- [10] Ribbe PH, Gibbs GV (1971) The crystal structure of topaz and its relation to physical properties. *Am Mineral* 56:24–30
- [11] Ribbe PH, Rosenberg PE (1971) Optical and X-ray determinative methods for fluorine in topaz. *Am Mineral* 57:168–187
- [12] Akizuki M, Hampar MS, Zussman J (1979) An explanation of anomalous optical properties of topaz. *Min Mag* 43:237–241
- [13] Zemmann RY, Zobetz E, Heger G, Vollenke H (1979) Strukturbestimmung eines OH-reichen Topases. *O<sup>sterreichische Akad Wiss Mathem Naturwiss Klasse</sup>* 116:145–147
- [14] Parise JB, Cuff C, Moore FH (1980) A neutron diffraction study of topaz: evidence for lower symmetry. *Min Mag* 43:943–944
- [15] Ribbe PH (1982) Topaz. In: Ribbe PH (ed) *Orthosilicates*, 2nd edn, vol 5. *Reviews in mineralogy*, Mineralogical Society of America, Washington, pp 215–230
- [16] Barton MD (1982) The thermodynamic properties of topaz solid solution and some petrological applications. *Am Mineral* 67:956–974
- [17] Barton MD, Haselton HT Jr, Hemingway BS, Kleppa OJ, Robie RA (1982) The thermodynamic properties of fluor-topaz. *Am. Mineral* 67:350–355

- [18] Northrup PA, Leinenweber K, Parise JP (1994) The location of H in the high-pressure synthetic  $\text{Al}_2\text{SiO}_4(\text{OH})_2$  topaz analogue. *Am. Mineral* 79:401–404
- [19] Wunder B, Rubie DC, Ross CR, Medenbach O, Seifert F, Schreyer W (1993) Synthesis, stability, and properties of  $\text{Al}_2\text{SiO}_4(\text{OH})_2$ : a fully hydrated analogue of topaz. *Am Mineral* 78:285–297
- [20] Wunder B, Andrut M, Wirth R (1999) High-pressure synthesis and properties of OH-rich topaz. *Eur J Mineral* 11:803–813
- [21] Alberico A, Ferrando S, Ivaldi G, Ferraris G (2003) X-ray singlecrystal structure refinement of an OH-rich topaz from Sulu UHP terrane (Eastern China)—structural foundation of the correlation between cell parameters and fluorine content. *Eur J Mineral* 15:875–881
- [22] Chen J, Lager G (2005) High-pressure infrared and powder X-ray study of topaz-OH: Comparison with hydrous magnesium silicate (humite). COMPRES 4th annual meeting, Mohonk Mountain House, New Paltz, NY, 16–19 June 2005
- [23] Chen J, Lager GA, Kunz M, Hansen T, Ulmer P (2005) A Rietveld refinement using neutron powder diffraction data of a fully deuterated topaz,  $\text{Al}_2\text{SiO}_4(\text{OD})_2$ . *Acta Cryst E* 61:i253–i255
- [24] Skinner BJ (1966) Thermal expansion. In: Clark SP (ed) *Handbook of physical constants*. Geol Soc Am Mem, pp 75–95
- [25] Komatsu K, Kuribayashi T, Kudoh Y (2003) Effect of temperature and pressure on the crystal structure of topaz,  $\text{Al}_2\text{SiO}_4(\text{OH}, \text{F})_2$ . *J Mineral Petrol Sci* 98:167–180
- [26] Birch F (1947) Finite elastic strain of cubic crystal. *Phys Rev* 71:809–824
- [27] The effects of F-OH-Substitution on the crystal structure of pegmatitic topaz Madison Barkley Mount Holyoke college.
- [28] Nuclear spin-lattice relaxation mechanisms in kaolinite confirmed by magic-angle spinning, Shigenobu Hayashi, Etsuo Akiba, Solid state, nuclear magnetic resonance, Received 28 November 1994; accepted 3 January 1995
- [29] “Nuclear Spin-lattice relaxation in Delute Paramagnetic Sapphire”, W.W. Simmons, W.J. O’Sullivan and W.A. Robinson, *Physical review*, vol.127, number 4, aug 15, 1962.
- [30] P-G de Gennes, *J. Phys.Chem. Solid* 7, 345 (1958)
- [31] Hoover, D.B. *Topaz*. Oxford: Butterworth-Heinemann Ltd, 1992
- [32] ) Local structure analysis of smoky and colorless topaz using single crystal  $^{27}\text{Al}$  NMR. Motohiro Mizuno *Journal of Physics and Chemistry of Solids* 67 (2006) 705–709
- [33] Singh D. 1991, *Phys.Rev.* B43, 6388
- [34] Sjostedt E, Nordstrom L and Singh D. J. 2000 *Solid State Commun.* 114, 15
- [35] Madsen G. K. H., Blaha P, Schwarz K, Sj .ostedt E and Nordstr .om L 2001, *Phys. Rev.* B64, 195134